ATTACHMENT 9

Westinghouse WCAP-17330-NP, Revision 0

(Non-Proprietary)

Westinghouse Non-Proprietary Class 3

WCAP-17330-NP
Revision 0

November 2010

H*: Resolution of NRC Technical Issue Regarding Tubesheet Bore Eccentricity (Model F/Model D5)

Westinghouse

WCAP-17330-NP
Revision 0

H*: Resolution of NRC Technical Issue Regarding Tubesheet Bore Eccentricity (Model F/Model D5)

W.J. Bedont*
SG Management Programs

C.D. Cassino*
SG Management Programs

A.O. Roslund*
SG Management Programs

G.W. Whiteman *
SG Management Programs

November 2010

Reviewer: **H.O. Lagally***
SG Management Programs

Approved: **D.A. Testa*, Manager**
SG Management Programs

**Electronically approved records are authenticated in the electronic document management system.*

Westinghouse Electric Company LLC
1000 Westinghouse Drive
Cranberry Township, PA 16066

TABLE OF CONTENTS

LIST OF TABLES

LIST OF FIGURES

1 INTRODUCTION

The purpose of H* is to replace the tube-end weld with the hydraulic expansion joint as the primary pressure boundary in the SG. There are two principal requirements for H*:

1. Assure that the tube(s) do not pull out of the tubesheet under the most limiting loads during normal operating or accident conditions.

2. Assure that the primary coolant leakage through the tube-to-tubesheet crevice is no greater than the leakage assumed in the final safety analysis report (FSAR) for the most limiting accident.

In October 2009, the NRC issued its first of several approvals of H*(Reference 1-1, typical). The approval in each case was limited to the operating period until the plant's next scheduled inspection because, as stated by the NRC, one technical issue remained to be resolved. The technical issue revolves around the relationship between tubesheet bore eccentricity and the tube-to-tubesheet contact pressure. This issue was identified in Reference 1-2, which provided 14 questions related to this issue. (Although Reference 1-2 is not a formal request for additional information (RAI), it will be referred to in this report as an RAI.) The purpose of this report, in conjunction with References 1-6 and 1-7, is to provide final resolution of the remaining questions in support of the permanent application of the H* criterion. The remaining eccentricity issue impacts both the structural and leakage analysis aspects of the H* analysis.

In this report, reference to the "current licensing basis" means the basis on which the temporary licenses were provided to the Model F and Model D5 plants. Principally, the technical basis for the current licensing basis is contained in WCAP-17071-P, Revision 2 (Reference 1-3) and WCAP-17072-P (Reference 1-4), but also includes other documents included in the respective License Amendment Requests (LARs) from the respective Model F and Model D5 plants.

1.1 ORIGINAL NRC RAI RESOLUTION ACTION PLAN DISCUSSION

Westinghouse initially interpreted the thrust of the questions as follows:

The H* structural justification includes an analysis that determines the contact pressure between the tubes and the tubesheet. The reference model for this calculation, the "Scale Factor Model" (SF) is a previously documented model (Reference 1-5) developed to determine the contact pressure for various values of dilation and eccentricity of the tubesheet bore. The output of this model is a multiplier to be applied to the calculated value of contact pressure due to tubesheet bore dilation, which is subtracted from the contact pressure generated due to tube-to-tubesheet differential thermal and pressure expansions. Because the transient conditions for one model (D5) of the affected steam generators required application of this model for conditions outside of the applicability of the reference model, a second model, the "Square-Cell Model" (C^2), a 2-D finite element analysis (FEA), was utilized to directly determine the contact loads between the tubes and the tubesheet for these conditions.

Both models are based on conservative analysis and assumptions; however, Westinghouse believes that the C^2 model more accurately represents the physical structure. Originally, the principal purpose of the C^2 model was to demonstrate that adequate contact pressure exists around the circumference of the tube under significant tubesheet bore eccentricity conditions. The two models, SF and C^2, are entirely

different approaches; thus it is not expected that the results from both models provide the same results. Westinghouse believed that, in aggregate, the NRC unresolved issue questions requested a comparison of the models and rationalization of the conservatism of the current licensing basis.

During a meeting in January 2010 with the NRC and the industry participants, Westinghouse proposed a plan to resolve all of the NRC questions through an approach believed to minimize the potential for additional questions. The NRC staff did not reject the recommended approach but stated that the 14 questions provided by Reference 1-2 must be clearly, if not directly, addressed. The target date established for a permanent H* license was the Spring 2011 outages. It was expected at the time that the contact pressures developed using the C^2 model would be of such a magnitude that the conservatism of the original licensing basis from both a structural and leakage integrity basis would be readily demonstrated.

1.2 REVISED NRC RAI RESOLUTION ACTION PLAN DISCUSSION

The Westinghouse action plan to respond to the 14 RAI questions was revised as discussed below.

1.2.1 Road Map to Final Response to 14 NRC RAI Except RAI # 5 and RAI# 12

It was determined by the NRC staff that the issues related to the SF model were resolved and that within the context of the SF model, eccentricity does not appear to be a significant variable affecting the tube to tubesheet contact pressure or calculated H* distances. This conclusion is based largely on the information provided in References 1-6 and 1-7 (LTR-SGMP-10-78 P-Attachment and LTR-SGMP-10-33 P-Attachment). From this information, the NRC staff concluded in Reference 1-8 that several of the NRC questions no longer require specific answers. Reference 1-7 provides a final response for each of the 14 remaining questions except RAI Questions # 5 and #12, which address the C^2 model specifically. A more detailed description of the C^2 model, necessary to complete this remaining action, is provided by this report.

1.2.2 Need for Alternate Leakage Factor Approach

The Darcy formulation was used in References 1-3 and 1-4 to develop the ratio of leak rates between postulated accident induced conditions (SLB/FLB) and normal operating conditions (NOP). The driving heads (Δp) at both of these conditions are known, as are the temperatures and pressures to define the fluid viscosity (μ). In References 1-3 and 1-4, because the physical length of the leak path was the same under both normal operating and accident conditions, the length of the leak path was not a factor. The only remaining factor was the loss coefficient (K). Based on the analyses using the C^2 model, the length of the leak paths under normal operating conditions and accident conditions may differ; therefore, the SLB:NOP leak rate ratio is re-evaluated in Section 4 of this report.

The available data for hydraulically expanded tubes in tubesheet simulants (References 1-9 and 1-10), both at room temperature and at elevated temperature, were used in Reference 1-3 and 1-4 to show that no correlation between loss coefficient and contact pressure. However, because the data exhibit considerable scatter, confidence in this data analysis was low. Engineering judgment could suggest that loss coefficient might be related to the absolute contact pressure between the tubes and the tubesheet. Hence, a requirement was applied to the H* leakage analysis by the regulatory authorities that it is necessary to

show that the contact pressure at accident induced conditions exceeds the contact pressure at normal operating conditions (Pc_{SLB}:Pc_{NOP}>1).

The calculated contact pressure results for all models of SG are, to a large degree, dependent on the temperatures at a particular operating condition. The limiting accident leakage condition for H* for the Model D5 SGs is the feedwater line break (FLB) condition. However, the limiting accident condition for the structural analysis of the Model D5 SGs is the steam line break (SLB) condition. The licensing basis for the Model D5 SG includes a SLB condition that differs from the SLB conditions in the licensing basis for the other SG models. The Model D5 SG SLB transient includes a significantly lower temperature; as a result, it cannot be shown that the contact pressures at accident conditions exceed those at normal operating conditions, and the criterion for contact pressure (Pc_{SLB}:Pc_{NOP}>1) is not met in application of the C^2 model as well as the SF model . Consequently, it was necessary to utilize a different approach for leakage analysis that does not depend on loss coefficient being independent of contact pressure to show that the accident induced leakage value assumed in the FSAR is not exceeded. Two alternate leakage methods were discussed in Reference 1-11, which are summarized in Section 4 of this report for completeness.

1.2.3 C2 Model Contact Pressures Results

Although in general, the C2 model contact pressure results exceed those based on the scale factor (SF) model results, the contact pressure results based on the C^2 model are not always greater than the scale factor (SF) model results. Using the C^2 Model. It was determined that the magnitude of contact pressures did not increase at all tubesheet radii at all elevations relative to the SF analysis results during normal operating and SLB conditions. As a result of the change in contact pressures, re-calculation of the probabilistic H* value was required for each model SG in the H* fleet.

1.2.4 Process for Determining the Limiting H* Value

The final H* depth recommended is the 95% probability at 50% confidence (95/50) estimate of H*. Consistent with prior practice, the 95% probability at 95% confidence (95/95) estimate of H* is also provided for information. The probabilistic H* depth is based on the mean H* value for the limiting tubesheet radius. As discussed in detail in References 1-3 and 1-4, the principal variables affecting the probabilistic value of H* are the coefficients of thermal expansion of the tube and tubesheet materials. The specific values of these variables that define probabilistic analysis of H* based on the C^2 model are determined from the variability surface described in Figure 8-5 of References 1-3 and 1-4. Application of these values in the C^2 model is discussed in Section 3.4 of this report. The probabilistic estimate of H* is further adjusted by the addition of a factor to account for the Poisson contraction of the tubes due to end cap loading, and a further adjustment of the length to account for the effect of the crevice pressure distribution which is dependent on the initially predicted length of H*. The adjustment for crevice pressure distribution is discussed in References 1-3 and 1-4 and Section 3.4 of this report. The adjustment for Poisson contraction is discussed in Section 3.5 of this report.

The limiting H* estimate for NOP, SLB and FLB is determined for the worst case sector of the tubesheet, which is the region of the tubesheet perpendicular to the tube lane, plus or minus five degrees azimuthally (see Section 6.2.3 of References 1-3 and 1-4). The H* estimate is determined using TS displacements from the worst case calculated using a 3-D half-symmetry finite element model of the

lower SG complex described in Section 6.2.1 of References 1-3 and 1-4 and further discussed in Section 3.2 of this report. The tubesheet displacements are input to the calculation of contact pressure between the tube and the tubesheet at nine elevations at each tubesheet radius in the limiting sector. The distribution of contact pressure as a function of elevation at a given tubesheet (TS) radius (see Section 3.3) defines the pull out resistance of a SG tube to an applied end cap load at that radius. The required H* length is defined by the integration of the cumulative pull out resistance as a function of depth in the tubesheet. The structural model used to calculate the contact pressures between the tubesheet and the tube is a pseudo sub-model to the 3D FEA model, called the square cell model (C^2 in this report). The C^2 model which is a quarter symmetry model of the tube and tubesheet material in a single tube pitch subjected to applied pressure and temperature in addition to the applied displacements from the tubesheet. A separate C^2 model is developed for each elevation at a single TS radius. The radial location of the worst case H* estimate is the TS radius with the longest required engagement length to balance an end cap load of $3\Delta P_{NOP}$ or $1.4\Delta P_{DBA}$ (whichever condition results in a greater H* value) assuming mean material properties. See Section 3.3 of this report for a detailed description.

The probabilistic estimate of H* is based on a Monte Carlo simulation for determining the effect of varying the TS coefficient of thermal expansion (CTE) and the tube (T) CTE on the contact pressure based on the limiting operating condition from the mean material estimate of H*. The final result of the simulation is the combination of TS and T CTE which defines the 95 percentile probability at a 50 percent or greater confidence estimate for increasing H* during the limiting operating condition at the limiting TS radius. The predicted combination of CTEs from the simulation is input to the C^2 model to calculate the value of H* at the required probabilistic estimate. See Section 3.4 of this report for a detailed description.

The distribution of contact pressure for the limiting operating condition, at the limiting TS radius, at the required probabilistic estimate, is used to determine the effect of Poisson contraction on the probabilistically defined H* value. The effect of Poisson contraction is determined by using standard thick shell equations (see Section 3-5) to calculate the reduction in contact pressure from a corresponding reduction in the outer diameter of the tube due to an applied axial end cap load on a closed thick walled pressure vessel. The net result is added to the probabilistic H* value to increase the required engagement length of the tube portion within the tubesheet. The Poisson contraction is based on the probabilistic contact pressure profile because the probabilistic value of H* is the basis of the requested license amendment. The crevice pressure effect is added to H* after the probabilistic value of H* with the Poisson effect is determined. The effect of crevice pressure on the structural analysis is described in Sections 6.4.8 and 8.1.2 of References 1-3 and 1-4 and in Section 3.4 of this report. The crevice pressure adjustment is applied after the adjustment for Poisson contraction because the Poisson contraction is an adjustment for a loading condition that is independent of the crevice pressure correction.

As a result of the issues discussed above, the action plan shifted from demonstrating the conservatism of the current licensing basis to the following:

1. Using the more accurate C^2 Model to confirm that the contact pressures at accident conditions exceed those at normal operating conditions, and to demonstrate that the criterion for contact pressure (SLB:NOP>1) for each of the Model SGs in the H* Fleet is met at all tubesheet bundle radii. For the Model D5 SG and for the 2 loop Model 44F SG, it was determined that the requirement $Pc_{SLB}:Pc_{NOP}>1$ could not be met; therefore, two alternate means were developed to

demonstrate that the leakage factors in place in the current licensing basis remain conservative for these model SGs.

2. Using the more accurate C^2 model, calculation of revised probabilistic H* values for each of the models of steam generators in the H* fleet.

Three reports will be completed for the entire population of H* candidate plants:

- a combined report for the Model F and D5 SGs (e.g., this report)
- a combined report for the Model 44F and 51F (3-loop plants)
- a separate report for the single Model 44F 2-loop plant

This report addresses the C^2 Model results for the Model F and D5 SGs and provides a final response to RAI Question Numbers 5 and 12. The remainder of the NRC RAI has been answered in previous submittals as discussed in Section 1.2.1 above.

1.3 REFERENCES

1-1. USNRC Letter, "Vogtle Electric Generating Plant, Units 1 and 2, Issuance of Amendments Regarding Technical Specifications (TS) Section 5.5.9, "Steam Generator Program," and TS 5.6.10, "Tube Inspection Report," for Interim Alternate Repair Criteria (TAC Nos. ME1339 and ME1340)," September 24, 2009.– (typical for H* participants)

1-2. USNRC Letter, "Vogtle Electric Generating Plant, Units 1 and 2- Transmittal of Unresolved Issues Regarding Permanent Alternate Repair Criteria for Steam Generators (TAC Nos. ME1339 and ME1340)," November 23, 2009.

1-3. WCAP-17071-P, Revision 2, H*: Alternate Repair Criteria for the Tubesheet Expansion Region in Steam Generators with Hydraulically Expanded Tubes (Model F), September 2010.

1-4. WCAP-17072-P, Revision 0, H*: Alternate Repair Criteria for the Tubesheet Expansion Region in Steam Generators with Hydraulically Expanded Tubes (Model D5), May 2009.

1-5. SM-94-58, Rev.1, "Doel 4 Elevated Tubesheet Sleeve – ASME Code Evaluation and Effect of Tubesheet Rotations on Contact Pressure," December 1995. (Proprietary)

1-6. LTR-SGMP-10-78 P-Attachment, "Effects of Tubesheet Bore Eccentricity and Dilation on Tube-to-Tubesheet Contact Pressure and their Relative Importance to H*," September 2010.

1-7. LTR-SGMP-10-33 P-Attachment, "H*: Response to NRC Questions Regarding Tubesheet Bore Eccentricity," September 2010.

1-8. USNRC Letter, "Vogtle Electric Generating Plant – Audit of Steam Generator H* Amendment Reference Documents (TAC Numbers ME3003 and ME3004)," July 9, 2010.

1-9. CN-SGDA-03-119, "Calculation of Loss Coefficient for Model D5 Steam Generators," Westinghouse Electric Company LLC, June 2004.

1-10. STD-MCE-03-49, "Determination of Model D5 Tube-to-Tubesheet Leakage Resistance for H-star Program for CBE/DCE/DDP/TCX," November 4, 2003.

1-11. LTR-SGMP-10-95, Rev. 1, "H*: Alternate Leakage Calculation Methods for H* for Situations When Contact Pressure at Normal Operating Conditions Exceeds Contact Pressure at Accident Conditions," September 3, 2010.

2 SQUARE CELL (C^2) MODEL ANALYSIS

2.1 PURPOSE OF THE C^2 ANALYSIS

Figure 1-1 in the current licensing basis (Reference 2-1) defines the calculation process for H*. The foundation for all of the structural analyses is a global model of the lower tubesheet complex (called the 3-D FEA model) that provides the tubesheet displacements that are used to calculate tube-to-tubesheet contact pressures. In the current licensing basis for H*, based on the thick-shell equations, tubesheet displacements generated by the bending of the tubesheet from the primary-to-secondary pressure differential in the global 3-D model are applied directly to the inner diameter of the tubesheet tube bore. This is a very conservative assumption that does not accurately represent the real physical condition. The deflections of the tubesheet tube bore surfaces occur due to the radial thermal growth, radial pressure growth and the primary-to-secondary pressure differential acting on the tubesheet. The thermal growth of the tubesheet itself and the distortion of the tubesheet tube bore due to bending of the tubesheet under the primary-to-secondary pressure differential are transmitted to the tube bore through the tubesheet material to the ligament surrounding a given tube. The square cell model analysis (C^2) is a conservative, more accurate, approach to modeling the process by which the tubesheet deformations are transferred to an individual tube bore. Figure 2-1 and Figure 2-2 illustrate the differences between the two approaches.

In Figure 2-1, the calculated local displacements must be applied to the inner diameter of the tubesheet tube bore. In Figure 2-2, the calculated local displacements are applied to the outer edges of the tubesheet cell material, and the displacements at the inner diameter of the tubesheet tube bore evolve from the local structural model (the C^2 model). The analysis method in Figure 2-2 is physically more realistic because it mimics the process by which the gross tubesheet displacements are transferred to the circumference of the tubesheet tube bore. The analysis method in Figure 2-1 is the simplest option for comparing the finite element model to analytical equations, i.e., the classical thick-shell equations. Also, if the geometry of the model is circular, the simplest way to apply a postulated load or displacement on the collars is to a surface which includes the inner diameter. However, because the global model does not include a distinct representation of the individual tube bore, additional assumptions must be made to determine what displacements should be applied to the boundaries of a local model (as shown in Figure 2-2) so that the tubesheet tube bore deflects in a realistic fashion.

The issue of how tubesheet tube bore deflection affects the tube-to-tubesheet contact pressure is the same regardless of the method chosen to apply displacements from the large scale model (3-D FEA) to the local sub-model. The basic problem is defined by how the large scale tubesheet deflections are transferred (or "mapped") to the local scale of a single tubesheet tube bore and tube. For the purposes of this report, the terms large scale and global scale refer to the 3-D finite element model of the channelhead, tubesheet, divider plate and lower shell (a.k.a., "Stub Barrel") that make up a typical Westinghouse designed steam generator in the existing domestic fleet (see Figure 2-3). In the case of the prior H* analysis (Reference 2-1), the sub-modeling is complicated by the fact that the presence of the perforations in the tubesheet are smeared throughout the perforated region in the tubesheet using the method of Slot (Reference 2-2). This means that in the global model of the lower steam generator complex the tube bores do not exist although the effect of the perforations on the structure is accounted for with respect to pressure and temperature. This is a complication for the square cell model approach because the exact displacements around a tube pitch cannot be directly taken from the 3-D finite element model of the lower SG complex.

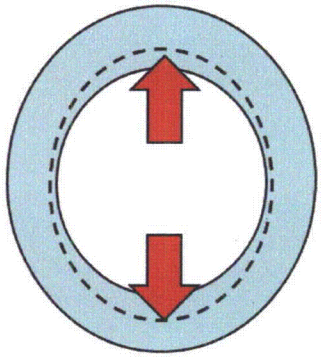

Figure 2-1 Current Licensing Basis Tubesheet Bore Displacements
(local displacement applied directly to tubesheet bore)

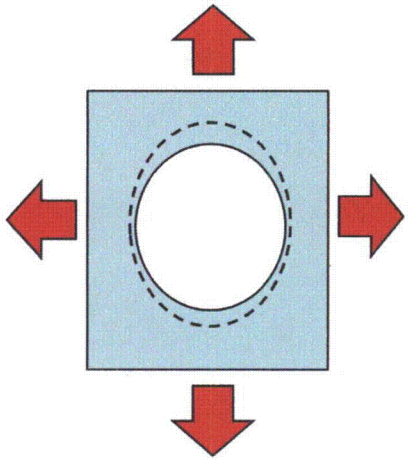

Figure 2-2 C^2 Model Tubesheet Bore Displacements
(local displacement applied to surrounding tubesheet material)

The effect of the perforations in the non-perforated model with the effective material properties includes the expansion of the tubesheet with respect to temperature and pressure, assuming that all the tubes in the bundle are pressurized. The elastic modulus and Poisson's ratio of the perforated material are altered so that the isotropic material becomes orthotropic. This means that the stiffness of the tubesheet along different axes is different so that the expansion of the tubesheet due to the combined pressure and temperature loads is conserved without the perforations being modeled. The question remains as to how to include the effect of the individual tube bores interacting locally. That question can be accommodated using different sub-models which, in general, are not necessary to calculate the tube-to-tubesheet contact pressure. Section 6.2.3 in Reference 2-1 describes one approach to bridging the gap between a single

tubesheet tube bore in an isolated model and including effects for the presence of other linked tubesheet tube bore at a local scale due to pressure at a given operating temperature. The reason they are not necessary is that along any given radial line from the center of the tubesheet it is possible to determine what the displacement is over that entire distance. This means that the displacement of a unit section can be determined but the displacement of a specific tube bore cannot be determined from the global model. In the case of H*, the displacement of specific tubes at key radii is used in determining the average tube-to-tubesheet contact pressure.

Figure 2-3 shows a general model of the lower steam generator complex which is the source of the displacements used in the square cell analysis. The intent of the C^2 model is to simulate a limited thickness "core sample" of a single tube at a given radius as shown in Figure 2-4. The square cell model, shown in Figures 2-5, 2-7, and 2-8, is a local model consisting of plane stress solid elements that approximate the tube and tubesheet material defined by a one-half tube pitch around a single tubesheet tube bore through the thickness of the tubesheet (typically 21.03 inches). This is the definition of the unit "square cell" model of the local tubesheet tube bore. The intent of this model is to provide a physically more realistic estimate of the contact pressure between the tube and the tubesheet at various elevations through the thickness of the tubesheet during the operating condition of interest.

2.2 DEFINITION OF THE C^2 MODEL

The square cell model is based on a unit cell of tubesheet material surrounding a single tubesheet tube bore in various models of Westinghouse steam generators. Each SG model is represented by a separate square cell model. The square cell is defined by taking one-half of the nominal tube pitch around a tube as the limit of the material in the model. The initial dimensions for the square cell model are based on the room temperature unpressurized condition. For example, in a Westinghouse model D5 SG, the tube pitch is [ ]^{a,c,e} inches. The outer nominal tube radius is [ ]^{a,c,e} inch. The inner nominal tube radius is [ ]^{a,c,e} inch. The resulting square cell is shown in Figure 2-6 below, with typical boundary conditions applied on the model. A quarter section of the model is typically used for analysis.

The square cell model is oriented in the X-Z plane of the tubesheet as defined in the lower SG complex shown in Figure 2-3. (For clarity, the square cell model is in the plane of the tubesheet but, for convenience, the square cell model is imported to ANSYS in an X-Y plane as noted in Figure 2-7.) The applied displacements, or forces, representing the net strain over the cell in the global X direction (formerly referred to in prior RAI responses as "e-bar") and the global Z direction (formerly referred to in prior RAI responses as "z-bar"). These net displacements are now referred to as ΔX and ΔZ.

[ ] a,c,e

Figure 2-3 Typical Lower SG Complex Model

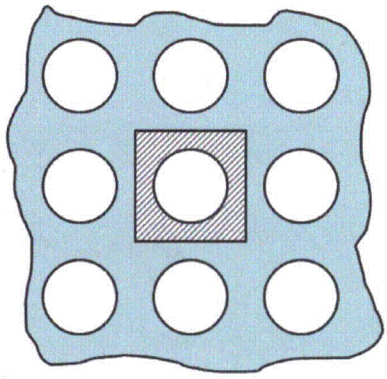

Figure 2-4 Square Cell Model "Core Sample"

[ ] a,c,e

Figure 2-5 Square Cell Model


a,c,e

Figure 2-6 Typical Square Cell Coordinate System


a,c,e

Figure 2-7 Typical Square Model without Symmetry Conditions

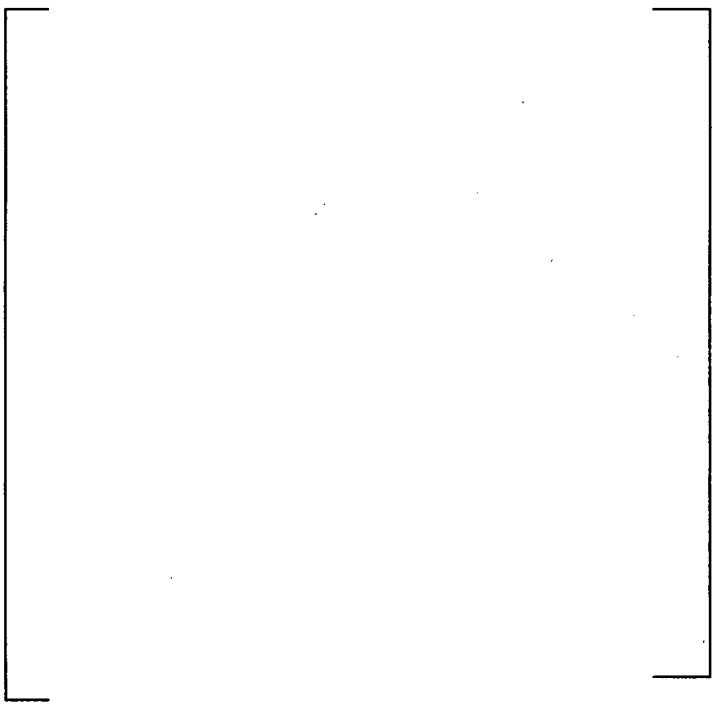

(a) Coarse Mesh

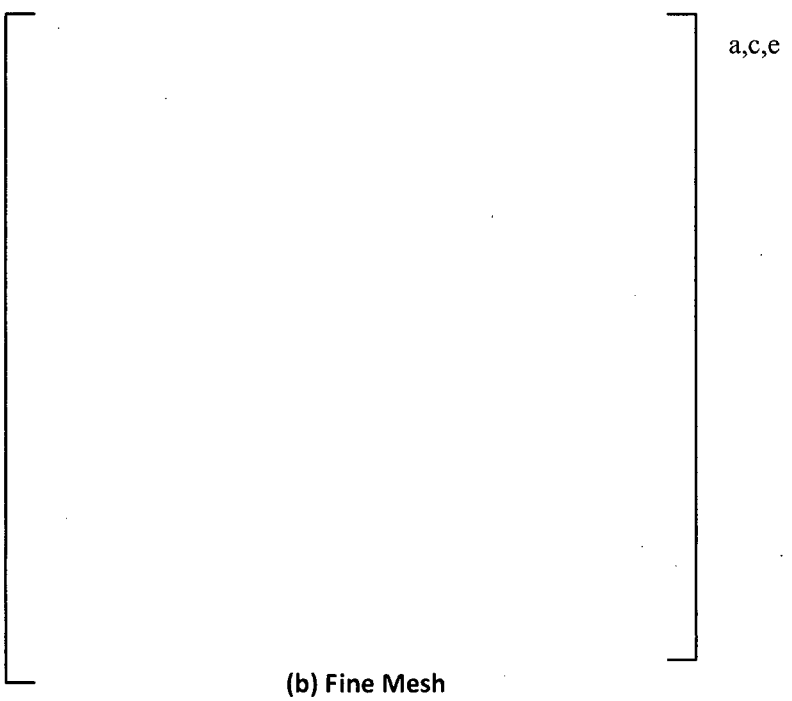

(b) Fine Mesh

Figure 2-8 Typical Mesh Square Cell with Quarter Symmetry Conditions

2.3 APPLICATION OF BOUNDARY CONDITIONS

There are three categories of boundary conditions that are applied in the square cell model: thermal, pressure and displacement. All components in the square cell model are assumed to be at a uniform temperature, depending on the operating condition, with the tube in equilibrium with the primary fluid temperature. The approaches taken in this analysis were selected because they are consistent with the current licensing basis for H*. The discussion below summarizes the issues with each approach to applying the pressure and displacement loads to the square cell model. The impact of any installation effects from the hydraulic expansion of the tube into the tubesheet tube bore is ignored in this analysis in order to be consistent with the licensing basis used for H*. The potential effect of any strain hardening from the expansion process can be ignored because the calculated elastic stresses in the tubes do not exceed the elastic limit of the tube material (see Section 6.2.5 of Reference 2-1).

2.3.1 Deformation of Tubesheet Cell Edges

Displacement based boundary conditions are used in the C^2 approach in a pseudo sub-model approach because the global model dictates how the sub-model should behave at the nodal level. For example, if the displacements due to the effect of temperature and pressure around the entire boundary of the sub-model are known, then those displacements can be directly applied to the sub-model. The square cell analysis is not a true sub-model analysis because the nodal displacement is not used as the applied boundary conditions. Instead, the average displacements over a tube pitch at a specified location and elevation are used. Loads which lead to additional displacements in the C^2 model (such as the thermal expansion of the tubesheet tube bore inner diameter) are not additive with the displacements from the initial conditions taken from the global SG model. This is because the applied displacements on the boundaries of the square cell model already account for the expansion of the tubesheet material due to pressure and temperature.

The preferred approach in the square cell analysis is to specify displacements at the boundaries of the tubesheet material as taken from the 3-D finite element model of the lower SG complex. Figure 2-9 illustrates the potential responses to the applied displacement that can occur in the square cell model.

It is important to understand that from the perspective of calculating the tube bore eccentricity based on the deflection of the major and minor axes of the tube bore all of the possibilities in Figure 2-9 (a through c) are equal. The reaction of the model to those displacements is different based on the nodal constraints are applied. For example, in Figure 2-9a, all nodes on the boundaries are assumed to expand equally along the different axes. In Figure 2-9b, nodal constraints are used so that the end points of the tubesheet material deform the entire distance and the remainder is linearly related to the maximum displacement. In Figure 2-9c, the displacement of the two surfaces in the model develops naturally based on the applied displacement with no constraints on the nodal behavior. Figure 2-9a represents the most conservative application of the displacement because it minimizes contact forces. Figure 2-9b will tend to maximize the eccentricity in the tubesheet tube bore but it is not likely that the outer edges of the tubesheet material will deform in this manner. This is because the growth in the tubesheet is mainly due to thermal effects which are nearly uniform in both directions and the growth from adjacent pressurized tubesheet tube bore will also act to prevent such a deformation in the majority of the bundle. Figure 2-9c has no assumptions on the deformation of the tubesheet tube bore material and allows a non-uniform displacement to develop on either edge in response to the applied displacement. However, the majority of the deformation in the

tubesheet is due to thermal effects, which means that the tubesheet material should deform in a mostly uniform manner. Therefore, the approach shown in Figure 2-9c is not used. Figure 2-9a is the preferred approach to applying the displacement taken from the lower SG complex model because it is the most conservative from an H* length perspective.

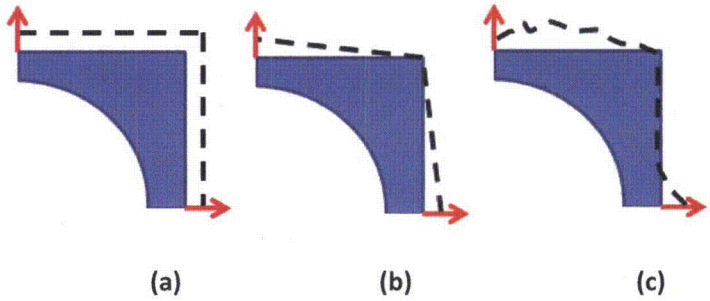

Figure 2-9 Sketches of Possible C^2 Model Response to Applied Displacement

2.3.2 Applying the Internal and Crevice Pressures in the Square Cell Model

Two pressure loads must be accounted for in the square cell model. The first is the internal pressure acting on the inner diameter of the tube representing the reactor coolant pressure. The second is the crevice pressure that the outer diameter of the tube and the inner diameter of the tube bore are exposed to assuming a throughwall flaw in the tube. The distribution of the crevice pressure varies according to the elevation of the tube in the tubesheet relative to the location of the flaw that allows the primary coolant into the crevice (References 2-3 and 2-4).

The internal pressure and crevice pressure can be included in the square cell model in two ways: First, the difference in the pressure acting on the outer diameter of the tube and the inner diameter of the tube can be applied as a pressure load that varies according to the elevation within the tubesheet. In this case, both the internal pressure acting on the tube and the crevice pressure are combined into the single differential pressure applied on the inner diameter of the tube. Second, the full internal pressure is applied to the inner diameter of the tube and the full crevice pressure (as a function of elevation) is applied to the outer diameter of the tube and the inner diameter of the tubesheet tube bore. The first option is the preferred approach in the square cell model because it conservatively minimizes the growth of the tube at the lower elevations of the tubesheet. This leads to a reduced contact pressure at the bottom of the tubesheet. This option is also simple to resolve with the contact options available in the structural analysis code, *ANSYS*, because a uniform pressure is pushing the outer surface of the tube into the inner surface of the tubesheet. The second crevice pressure option is difficult to resolve with the contact options in *ANSYS*.

The crevice pressure is assumed to act on 100% of the circumference of the outer diameter of the tube surface and inner diameter of the tubesheet tube bore. It is also simpler to account for the effect of the crevice pressure over the entire tubesheet tube bore as opposed to limited regions of the tube outer diameter. This assumption is conservative because test data (References 2-1 and 2-4) shows that this cannot occur. The observed leakage during the tests was more aptly characterized as "weepage," i.e.,

dropwise leakage. Also, recent work reported in the literature (Reference 2-5) based on fluid structure interaction shows that fluid blanketing of the entire crevice cannot occur. Both point to evidence that supports the assumption in the analysis of record for H* of a "tortuous path" that the liquid must take as it diffuses through the porous medium of the tube-to-tubesheet crevice. However, the nature of the test specimens, used in References 2-1 and 2-4, make it impossible to ascertain what portion of the tube outer diameter constitutes a wetted surface. Limited sensitivity studies have been performed to determine the effect of applying the crevice pressure over a smaller portion of the tube. In these studies, "bubbles" of crevice pressure were applied to the tube bore inner diameter and the tube outer diameter while the full internal pressure was applied to the inner diameter of the tube. The "bubbles" varied in circumferential extent from 10 to 75 percent of the tube outer diameter. The effect of limiting the crevice pressure to less than 100 percent of the outer tube diameter was an increase in the average tube to tubesheet contact pressure of at least 10 percent.

2.4 DISCUSSION OF MATERIAL PROPERTIES

The manufacturing process used to assemble a steam generator creates a strain hardened condition in the tubes. The tubes are initially inserted into the steam generator tubesheet tube bores, "tack" expanded into the tubesheet near the tube end by hydraulic (urethane plug) expansion or mechanical hard rolling over approximately a 0.75 inch length, and welded to the tubesheet. Each tube is then hydraulically expanded into contact with the tubesheet tube bore over the full depth of the tubesheet. This means that each of the tubes in the tube bundle begins in contact with the tubesheet tube bore. It also means that the tubes create a material non-linearity with respect to the contact pressure analysis because they are strain hardened to a small percentage (1 to 3 percent on average) and typically thinned to a small extent (~1% wall thinning). No non-linear material effects are present in the tubesheet tube bore material. Consistent with the basis of the current licensing basis, the square cell model ignores any effects that could benefit the contact pressure analysis that come from the tube installation and steam generator manufacturing process, including any strain hardening effect, residual contact pressure, wall thinning or other material non-linearity.

Test data has shown that the installation and tube expansion process develops sufficient pull out resistance between the tube and the tubesheet at room temperature and at elevated temperature conditions (Reference 2-1) to resist any applied pull out loads during normal and accident conditions. Any additional contact pressure due to tubesheet deformation or applied pressure is above and beyond what is already sufficient to prevent pull out of the tube portion within the tubesheet. Therefore, it is conservative and convenient to ignore strain hardening resulting from initial tube expansion as an initial condition. No elastic-plastic effects are included in the analysis. The displacements and pressures acting on the tubes are applied in an elastic analysis. This is appropriate provided that the average radial stress in the tube material due to the applied loads is less than [ ]^{a,c,e} ksi. None of the contact pressure results in the tube material for the square cell model described in this report approached an average radial stress of 30 ksi.

The material properties used for the tube and the tubesheet materials in square cell model are the same as originally used in the licensing basis analysis, Reference 2-1. The properties used for the Alloy 600 thermally treated tubing and SA-508 tubesheet materials are provided in Tables 3-2 and 3-4.

The Poisson's Ratio used for the tube material is [ ]^{a,c,e}. The Poisson's Ratio used for the tubesheet material is [ ]^{a,c,e}.

2.5 CONTACT MODELING DISCUSSION

The only boundary conditions that limit the displacement of the tube in the square cell model are the symmetry conditions on the edges of the model. This means that in the square cell model the contact between the tube and the tubesheet is what limits the potential displacement of the tube. If the contact relationship between the tube and the tubesheet is modeled inappropriately, the tube in the model could slide past the tubesheet and experience rigid body translation. Another possibility is that the tube deformations could lead to inter-penetration of the tube material into the tubesheet material which would generate unrealistically high contact pressures. Conversely, if the contact law is determined to resist node to node contact too strongly, the results of the analysis would be an unrealistically low contact pressure. While the *ANSYS* solver is capable of using different numerical schemes to resolve these difficulties, it is up to the user to make sure that the results which are obtained are appropriate. In the application of the square cell model, the contact pressure results using different contact modeling options were compared to determine the best approach. The final contact model used in the square cell analysis is a frictional model which is consistent with the assumptions in the H* analysis (e.g., $\mu = [\quad]^{a,c,e}$).

The simplest way to prevent difficulties with a contact law is to construct a properly converged mesh. It is difficult for nodal interpenetration to occur if a mesh is fine enough, and the nodal positions on either side of the contact interface are aligned properly. Two mesh designs were evaluated in the C^2 analysis. Figure 2-8 shows the two meshing schemes of the model used in the analysis. The coarse mesh (shown in Figure 2-8a) has approximately [ ]^{a,c,e} contact elements along the tube-to-tube bore interface. The fine mesh (shown in Figure 2-8b) has approximately [ ]^{a,c,e} contact elements along the tube-to-tube bore interface. The fine mesh tends to predict an increase in the tube-to-tubesheet contact pressure relative to the coarser mesh and can resolve the contact pressure closest to the boundaries in a quarter symmetry model. However, the contact pressures nearest the displacement boundary conditions on the tube in the quarter symmetry model are not significant to the problem and lower contact pressures are conservative. Therefore, for conservatism, the preferred meshing scheme in the square cell analysis is a more coarse mesh. The actual mesh used in the final analysis is slightly less coarse than shown on Figure 2-8a.

The tubesheet is defined as the contact target body because the deformation of the tubesheet material is more controlled. The tube is defined as the contact body because the tube is expanding into the tubesheet material and its deformation is poorly controlled in the model. The contact relationship between the tube and the tubesheet is defined as symmetric and rough (e.g., with friction). The contact is symmetric for numerical expediency and because, in the range of deformations under consideration, the tube may lose contact with the tubesheet or the tubesheet may lose contact with the tube. The friction interface allows two-dimensional sliding between the tube and the tubesheet. Shear stresses can develop due to "stick-slip" behavior because the coefficient of friction between the tube and the tubesheet in this model is greater than zero. However, these shear stresses are separate from the calculated contact pressures in *ANSYS* and do not affect the final results used to calculate H*.

The augmented Lagrangian solver in *ANSYS* is used to resolve the contact so that the contact pressure results have a smaller variation around the circumference of the tube bore and because the extra degree of freedom helps the solver to calculate the contact interactions quickly. The tube and tubesheet are initially adjusted to be "just touching" using the contact options in *ANSYS*. The geometry defined in the model is such that the tube and tubesheet begin in line on line contact at the tube-to-tubesheet interface. However, the possibility exists for a small geometric inconsistency to lead to an interpenetration of the tube and

tubesheet materials. Therefore, the tube outer surface and tubesheet inner surface are separated by an initial offset of +0e00 inch in *ANSYS* to set the initial gap to zero and to assure that no interpenetration occurs. There are two options used in the analysis for managing the stiffness of the interface in the square cell model. The first option assumes that the stiffness of the interface is constant and does not need to be updated as the analysis proceeds to completion. This first option is the most similar to an analytical model using thick shell equations to solve for the contact pressure between the tube and the tubesheet. The second option assumes that the stiffness must be constantly updated to prevent interpenetration of the tube and tubesheet and adjust the contact law as the deformation of the nodes at the interface shift during the analysis. The "pinball" radius, the radius about a node, in which. if another existing node is recognized to be in contact, was set to [ ]^{a,c,e} inch to reflect the surface roughness of the post-expanded tube.

2.6 DISCUSSION OF BENCHMARK MODEL FOR C2 MODEL COMPARISON

The contact pressure results for the square cell analysis were benchmarked against classical thick shell equations. The thick shell model for the composite tube and tubesheet collar was developed to accept the displacement of the tubesheet inner diameter surface as input. The benchmark model used the Model D5 tube and tubesheet geometry. The benchmark model used a different thick shell model (see below) than described in the existing licensing basis for the calculation of the H* analysis contact pressures because the goal of the model was to provide an independent check on the square cell model results and the H* methodology.

2.6.1 Thick Shell Model to Describe Finite Element Model

The tube and tubesheet cylinders can be represented as two concentric, open cylinders. The tube material is thermally treated Alloy 600. The tubesheet material is SA-508 Class 2. Neither cylinder has an applied axial load. There is no internal pressure within the tube. The coefficient of friction between the inner diameter of the tubesheet and the outer diameter of the tube is zero. The tube and the tubesheet are held at the same constant temperature during the simulation of the operating condition although the tubesheet is assumed to have a coefficient of thermal expansion equal to zero. The tube bore dilation, or expansion of the inner tubesheet collar diameter, is specified in the analysis and assumed to be constant regardless of any applied loading for the tube. The tube and tubesheet cylinders are assumed to have a zero stress, or a constant stress condition, along the tube axis (e.g., σ_{ZZ} = 0 psi). The assembled model geometry appears in Figure 2-10.

In Figure 2-10, *a* is the inner radius of the tube, *b* is the outer radius of the tube and also the inner radius of the tubesheet tube bore, and *c* is the outer radius of the tubesheet collar.

The free radial expansion of the tube, due to a change in temperature, is given by:

$$\Delta R_{\Delta T} = \frac{OD}{2} \bullet \alpha_{TUBE}\left(t - t_{REF}\right) \qquad \text{(Equation 2-1)}$$

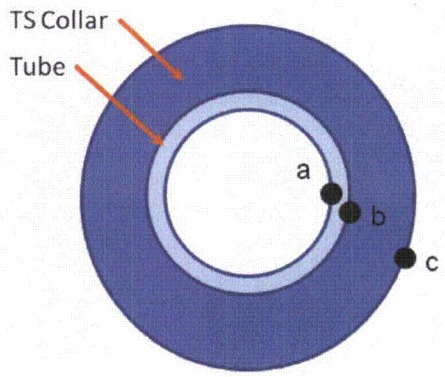

Figure 2-10 Tube and TS Collar Assembly.

Where OD is the outer diameter of the tube, α_{TUBE} is the coefficient of thermal expansion of the tube, t is the temperature of the tube and t_{REF} is the reference temperature in the analysis for the material of interest (typically 70°F). Several values of constant tubesheet tube bore inner diameter displacements were selected for the purposes of this sensitivity study. It is assumed that the tubesheet is essentially rigid with respect to any applied loading from the tube in excess of the initial dilation. The tube bore is assumed to deform (or dilate) as a perfect circular surface without any non-uniformities around the circumference of the tube. The difference between the specified tubesheet tube bore dilation and the amount that the tube wants to expand will create a contact stress between the tube and the tubesheet. See Figure 2-11.

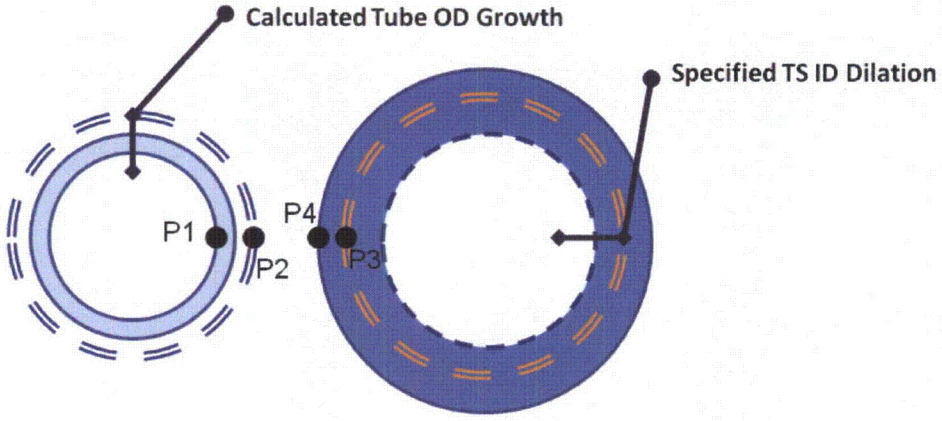

Figure 2-11 Constant Tubesheet Bore Dilation Model

In Figure 2-11, P1 is the internal pressure applied to the inner surface of the tube, P2 is the external pressure applied to the outer surface of the tube, P3 is the internal pressure applied to the inner surface of

the tubesheet collar, and P4 is the external pressure applied to the outer surface of the tubesheet collar. In the tube and tubesheet assembly, the contact pressure between the two cylinders is taken at the inner surface of the tubesheet collar and the outer surface of the tubesheet such that they are both equivalent (e.g., P2 = P3). There are no other applied pressures on the system so P1 = P4 = 0 psi.

The differential free radial expansion of the tube at normal operating conditions (NOP, t = [ ]^{a,c,e}°F) and steam line break conditions (SLB, t = [ ]^{a,c,e}°F), calculated using Equation 2-1 and the material properties defined in Table 3-3 and Table 3-4. The NOP operating temperature of [ ]^{a,c,e}°F was chosen to better compare to previous results in Reference 2-1 and is still representative of typical NOP conditions. The results are summarized in Table 2-1.

The difference between the inward radial dilation of the tubesheet tube bore and the outer diameter of the tube will change based on the temperatures during operation. The difference between the specified radial dilation of the tubesheet tube bore and the radial growth of the tube for each operating condition is shown in Table 2-2.

Column (1) in Table 2-2 is the assumed inner radius of the tubesheet tube bore and Column (2) in Table 2-2 is the amount that the tubesheet tube bore is allowed to dilate in the analysis. Column (3) and Column (4) in Table 2-2 are the difference between the allowed dilation in Column (2) and the results in Table 2-2 for each operating condition (e.g., ΔU_{NOP} = Tube Growth – Tubesheet Growth). The difference between the deformations is taken so that a positive value means that the tube deformation exceeds the growth allowed by the tubesheet collar

The equation for the radial deformation (either positive or negative) of the tube as an open thick walled cylinder at a constant temperature due to pressure loading is:

$$\Delta R_{TUBE} = \frac{r}{E_{TUBE}\left(b^2 - a^2\right)}\left[\left(1 - \nu_{TUBE}\right)\left(p_1 a^2 - p_2 b^2\right) + \frac{\left(1 + \nu_{TUBE}\right)a^2 b^2}{r^2}\left(p_1 - p_2\right)\right] \qquad \text{(Equation 2-2)}$$

Where r is the radial location within the tube material, b is the outer radius of the tube, a is the inner radius of the tube, E_{TUBE} is the Young's modulus of the tube at the given operating condition and ν_{TUBE} is the Poisson's Ratio for the tube material. The equation for the radial deformation (either positive or negative) of the tubesheet collar as an open thick walled cylinder at a constant temperature due to pressure loading is:

$$\Delta R_{TS} = \frac{r}{E_{TS}\left(c^2 - b^2\right)}\left[\left(1 - \nu_{TS}\right)\left(p_3 b^2 - p_4 c^2\right) + \frac{\left(1 + \nu_{TS}\right)b^2 c^2}{r^2}\left(p_3 - p_4\right)\right] \qquad \text{(Equation 2-3)}$$

Where r is the radial location within the tubesheet material, c is the outer radius of the tubesheet collar, b is the inner radius of the tubesheet collar, E_{TS} is the Young's modulus of the tubesheet at the given operating condition and ν_{TS} is the Poisson's Ratio for the tubesheet material.

The deformation of the tube is limited by the specified deformation of the tubesheet collar, as shown in Table 2-2, Columns (3) and (4). The values in Columns (3) and (4) are all positive; therefore, the final state of the tube outer surface and the tubesheet inner surface is positive contact. The magnitude of the

contact pressure between the tube and the tubesheet will be the result of the additional growth that the tube cannot release due to the "rigid" tubesheet collar. The equation for the change in radial position of the contact surface between the tube and the tubesheet is:

$$\Delta U = [\Delta R_{TS}]_{r=b} - [\Delta R_{TUBE}]_{r=b} \qquad \text{(Equation 2-4)}$$

Where ΔU is the condition specific result from Table 2-2 for the appropriate value of tubesheet collar dilation in Column (2). Setting P1 and P4 equal to zero and P2=P3 in Equation 2-2 and Equation 2-3 yields the following for r = b,

$$\Delta U = \frac{b}{E_{TS}\left(c^2 - b^2\right)}\left[\left(1 - \nu_{TS}\right)\left(p_2 b^2\right) + \frac{\left(1 + \nu_{TS}\right)b^2 c^2}{b^2}\left(p_2\right)\right] - \ldots$$

$$\ldots - \frac{b}{E_{TUBE}\left(b^2 - a^2\right)}\left[\left(1 - \nu_{TUBE}\right)\left(-p_2 b^2\right) + \frac{\left(1 + \nu_{TUBE}\right)a^2 b^2}{b^2}\left(-p_2\right)\right] \qquad \text{(Equation 2-5)}$$

Rearranging to solve for P2 gives the final result.

$$p_2 = \Delta U\left[\frac{b}{E_{TS}\left(c^2 - b^2\right)}\left[\left(1 - \nu_{TS}\right)\left(b^2\right) + \left(1 + \nu_{TS}\right)c^2\right] + \frac{b}{E_{TUBE}\left(c^2 - b^2\right)}\left[\left(1 - \nu_{TUBE}\right)\left(b^2\right) + \left(1 + \nu_{TUBE}\right)a^2\right]\right]^{-1} \qquad \text{(Equation 2-6)}$$

In this case the contact pressure is a kind of residual stress locked into the assembly by the restrictions on tube deformation.

Solving Equation 2-6 for each value in Column (3) and Column (4) in Table 2-2 with the properties in Table 2-3 and Table 2-4 yields the results shown in Table 2-5.

The results in Table 2-6 exclude any effect of non-uniform deformation around the circumference of the tubesheet tube bore. The loss of contact pressure between the tube and the tubesheet is due solely to the expansion (or dilation) of the tubesheet tube bore relative to the expansion of the tube due to thermal effects. Real deformations applied to the tubesheet tube bore are not perfectly uniform. Therefore, the displacement of the inner tubesheet tube bore was used in order to benchmark the model to compare directly against the C^2 model. Only the average tube to tubesheet contact pressure around the circumference of the tube can be calculated using the thick shell equation. This is an acceptable comparison to the finite element results because only the average contact pressure around the circumference of the tube is used in the calculation of H*. This benchmark was performed for the Model D5 NOP condition. The expansion of the inner surface of the tubesheet tube bore due to a pressure differential across the tube wall (i.e., the pressure of the primary fluid minus the assumed circumferentially uniform pressure in the tube/tubesheet crevice) and an applied temperature is shown in Table 2-6. This result was then applied to the inner diameter of the tubesheet surface in the C^2 model. The tube bore displacement in Table 2-6 varies as a function of elevation due to the change in the crevice pressure distribution. The result of using the calculated tubesheet tube bore displacements in the square cell and analytical models is given in Table 2-7. The average contact pressure between the tube and the tubesheet in the C^2 approach with the contact law as described is a very close approximation of the thick

shell equation for the same uniform tubesheet tube bore displacement. Based on the comparison with the thick-shell equation models, the C^2 approach and the modeling described in this section are reasonable and appropriate.

Table 2-1 Free Radial Expansion of a Tube

Condition	Nominal Tube OR	α_{TUBE}	T	t_{REF}	ΔR
	in	in/in-°F	°F	°F	in
NOP					
SLB					

a,c,e

Table 2-2 Difference Between Radial Dilation of the Tube Bore and Tube

(1)	(2)	(3)	(4)
Avg TS IR	Change in TS IR	ΔU_{NOP}	ΔU_{SLB}
in	in	in	in

a,c,e

Table 2-3 Rigid Collar Model Input Parameters (Tube)

Nominal Tube Properties			
Variable	Description	Value	Units
b	OR		in
a	IR		in
	E (NOP)		psi
	E (SLB)		psi
	α (NOP)		in/in-°F
	α (SLB)		in/in-°F
	Poisson's Ratio		-

a,c,e

Table 2-4 Rigid Collar Model Input Parameters (Tubesheet)

Nominal TS Properties			
Variable	Description	Value	Units
c	OR	[ ]a,c,e	in
b	IR		in
	E (NOP)		psi
	E (SLB)		psi
	a (NOP)		in/in-°F
	a (SLB)		in/in-°F
	Poisson's Ratio		-

Table 2-5 Rigid Collar Model Contact Pressure Results

(1)	(2)	(3)
Avg. TS IR	**P2 NOP**	**P2 SLB**
In	Psi	psi

[ ]a,c,e

Table 2-6: Calculated Tubesheet Inner Diameter Dilation

Thermal Expansion of TS ID		[ ]a,c,e	in
Tubesheet Elevation	ΔP_{CREV} Expansion	Combined Expansion	
BTS	[	]a,c,e	in
NA			in
TTS			in

Table 2-7: Comparison of C2 and Thick Shell Results

	Contact Pressure Results		
	TTS	NA	BTS
Max (psi)			
Min (psi)			
Average (psi)			
Thick Shell			

a,c,e

2.7 REFERENCES

2-1. WCAP-17072-P, "H*: Alternate Repair Criteria for the Tubesheet Expansion Region in Steam Generators with Hydraulically Expanded Tubes (Model D5)," May 2009.

2-2. *Stress Analysis of Thick Perforation Plates*, T. Slot, 1972.

2-3. LTR-SGDA-07-4 (Proprietary), "Letter Summary of Changes to B* and H* Analysis due to New Crevice Pressure and Divider Plate Data," Westinghouse Electric Company LLC, Pittsburgh, PA, January 17, 2007.

2-4. STD-MC-06-11-P, Rev. 1, "Pressure Profile Measurements During Tube-to-Tubesheet Leakage Tests of Hydraulically Expanded Steam Generator Tubing," Westinghouse Electric Company LLC, Pittsburgh, PA, August 30, 2007.

2-5. Journal of Pressure Vessel Technology, August 2006, Volume 128, Issue 3, pp 408-413.

3 STRUCTURAL CALCULATIONS FOR H*

Section 2 of this report provided a description of the C^2 model, its intent, its design, how it fits in the overall process for calculating the H* distance and what its capabilities are relative to the model based on the thick-shell equations. This section summarizes the actual analyses performed for the Model F and Model D5 SGs. Sections 3.1 through 3.3 summarize the significant assumptions in the application of the C^2 model, and the interface between the C^2 model and the 3-D FEA model of the lower tubesheet complex. Section 3.2 discusses the boundary conditions applied for the limiting Model D5 plant, Byron/Braidwood Units 2, and the boundary conditions applied for the limiting Model F plant, Millstone Unit 3. Section 3.3 discusses the solution for the mean value of H*, including the displacement inputs from the 3-D FEA model and the axial contact pressure profiles each tubesheet radius for both the Model D5 and Model F SGs in both tabular and graphical form. Section 3.4 provides the probabilistic analysis based on the C^2 model for the Model D5 and Model F SGs. By its design and its interface with the 3-D FEA model of the lower tubesheet complex, the C^2 model cannot directly include the effect of Poisson contraction on H*; however, section 3.5 provides the analysis of Poisson contraction on H* predicted using the C^2 model. In this section, Millstone 3 and Byron/Braidwood 2 are frequently discussed. Millstone 3 is the limiting plant for the Model F SG plants and Byron/Braidwood 2 are the identical limiting plants for the Model D5 SG plants. The criteria for defining the limiting plants are discussed in the current licensing basis (i.e., Reference 3-1 and 3-2).

3.1 OVERVIEW OF THE STRUCTURAL ANALYSIS FOR H*

As noted in Section 2.0 of this report, the C^2 model is a planar model of a tube in a tubesheet segment. The tubesheet segment can be visualized as a square local segment of the tubesheet that is defined by a single tube pitch ([ ]^{a,c,e} inches for the Model D5, [ ]^{a,c,e} inch for the Model F) centered on the location of a tube (see Figure 2-4). The model includes the tubesheet bore and a tube in its expanded diameter but without any residual contact pressure from the hydraulic expansion process. Thus, in its unloaded state, the tube is in zero-pressure line-on-line contact with the tubesheet bore.

The loading conditions applied to the square cell model are:

- temperature, which varies axially through the tubesheet
- the internal tube pressure modified by the axially-dependent crevice pressure
- planar displacements at the model boundaries, which are taken from the 3-D-FEA model of the tubesheet complex when it is loaded by temperature increase and differential pressures applicable to the operating conditions of interest

In the licensing basis analysis, when applying the thick-shell model, similar displacements were applied directly to the tubesheet bore; however, in the C^2 model application, the displacement conditions are applied to the boundaries of the model and the model determines the conditions at the actual tube-to-tubesheet interface. This is a key difference between the C^2 model and the thick shell model.

To calculate the axial contact pressure profile for a tube at the tubesheet radius of interest, the temperatures and displacements appropriate to nine points through the thickness of the tubesheet are input

separately to the model along with the tube-wall pressure differential between the internal pressure of the tube, and the crevice pressure acting on the outer diameter of the tube wall and inner diameter of the tubesheet applicable to each elevation to determine the contact pressure between the tube and the tubesheet at each elevation. The elevations through the thickness of the tubesheet are consistent with the elevations utilized in the current licensing basis for H*. Application of the C^2 model assumes that the centerline of the tube remains straight, e.g., that no bending of the tubesheet occurs. The displacement input conditions, taken from the 3-D FEA model of the tubesheet complex, include the total effects of temperature and pressure loading in the continuum of the thickness of the tubesheet. Ignoring the coupling due to tubesheet bending in applying the C^2 model is a very conservative application of this model because the introduction of tubesheet bore and tube bending would be expected to result in much higher contact pressures between the tube and tubesheet.

The input boundary conditions include displacements in both axes of the plane. Conceptually, this is similar to the original analysis using the thick-shell equations, but the application details are different. Previously, the radial displacement was taken directly from the 3-D FEA model, and the circumferential displacement was derived from the radial displacement (see Section 6.3 of WCAP-17072-P) and applied directly to the tubesheet bore. For application of the C^2 model, which is driven by the cell boundary displacements, it was desired that the radial displacements be calculated directly in the 3-D FEA model of the tubesheet complex. To facilitate this, the 3-D-FEA model was modified by adding the same mesh used on the tubesheet centerline face perpendicular to the divider plate one and two pitches into the depth (not thickness) of the tubesheet. This permitted obtaining the displacements in the direction parallel to the divider plate directly from the 3-D FEA model for application to the C^2 model boundaries instead of direct application to the tubesheet bore.

The 3-D FEA model mesh was also modified for other reasons not directly related to application of the C2 model. For example, to avoid applying a factor to account for a non-functional divider plate, the model was changed to directly reflect that the upper five inches of the divider plate were assumed to be non-existent (see Section 3.2.2). Further, changes were made to the 3-D FEA model mesh to properly represent the axial thermal profile through the thickness of the tubesheet (see Section 3.2.5).

3.2 STRUCTURAL ANALYSES (3-D FEA MODEL)

3.2.1 Method Discussion

The structural finite element analysis is based on a 3-dimensional (3-D) model of the lower steam generator complex consisting of the channelhead, divider plate, tubesheet, and lower shell. The model uses Slot's effective material properties to model the perforated tubesheet section as an orthotropic material, as discussed in References 3-1, and 3-2. The plants are analyzed for low T_{avg} normal operating conditions (NOP) and steam line break (SLB), which have been determined to be limiting conditions in References 3-1 and 3-2. Note that these conditions represent the bounding pressure and temperature values specified by the design basis transients and represent the design limits of the plant operating conditions but not the current actual plant operating conditions.

Because it was determined by consistent application of both the C^2 model and the thick shell model that the SLB condition is the limiting condition for H* for the Model D5 SGs, an analysis of the Model D5 SG was required using the 3-D FEA model to develop the SLB uncertainty surface to support the

probabilistic H* analysis. This analysis is consistent with the analysis methods documented in Reference 3-2. The results from the SLB 3-D FEA analysis for the Model S5 SGs, as documented in Reference 3-11, are utilized in Section 3.4 for the Model D5 probabilistic analysis.

3.2.2 Discussion of Significant Assumptions

The assumptions below, with the exception of the thermal temperature profile through the tubesheet, are copied from References 3-1 and 3-2. For each analysis condition, a thermal and a combined thermal-structural analysis were performed to determine the deformations in the tubesheet. All of the finite element analysis (FEA) results assume a static, steady-state, linear, and elastic system.

An analysis performed in Reference 3-3 concludes that, in general, the tubesheet is approximately at the primary side temperature through its thickness, except for a sharp thermal gradient that exists in approximately the top one (1.00) inch. In the thermal analysis, the secondary side of the tubesheet was assumed to be at a temperature equal to the average of the steam temperature and the feedwater temperature. The tubesheet portion of the 3-D FEA model used in this analysis was partitioned two (2.00) inches from the top of the tubesheet. From the bottom of the tubesheet to the top of this partition in the tubesheet, an approximately uniform temperature equal to the hot leg temperature was applied. This produced a temperature gradient in the top two inches of the tubesheet from a value of 10 degrees cooler than the primary fluid temperature to the average of the coldest allowable condition-specific feedwater and steam outlet temperatures as specified by the applicable PCWG (see Section 5 of References 3-1 and 3-2 for details). For the SLB case, the primary fluid and the average of the secondary fluids were applied to the primary and secondary surfaces of the tubesheet, respectively, so that a linear temperature gradient developed through the thickness of the tubesheet. This is a reasonable assumption because the long-term portion of the transient specifies that flow will be reduced to natural circulation through the affected loop when the reactor coolant pumps are off.

Where a range of feedwater temperatures was specified in the PCWG parameters, the condition most conservative for H* was used. Since H* values are negatively impacted (i.e., greater H* values result) by large radial deformations of the tubesheet, a higher overall temperature of the tubesheet will result in a lower modulus, and thus a conservative H* value.Note that only the tubesheet temperature is at issue here because the tube temperature remains at the design T_{hot} for the normal operating condition.

The transient analyses for SLB are performed statically. This results in a conservative H* value, because the maximum pressure and asymptotic temperature from the transient is used. It is reasonable to use a static analysis for the long-term conditions since these transients are very long and the steady-state portion of the transient continues for hours.

The dimensions used for the finite element model were consistent with the current licensing basis.

The finite element model did not include the nozzles or manways. This is reasonable because the deformations of interest are in the tubesheet, which is well removed from the channelhead penetrations, and thus, would not be expected to have a significant effect on tubesheet deflections. Prior analysis has shown that including the larger channelhead penetrations, such as the manways, tends to decrease displacements in the tubesheet. Decreasing tubesheet displacements will produce shorter H* distances; therefore, the current approach is conservative. The model did not consider the tubes or any of the

structure above the tubesheet except the lower shell (stub barrel). Including the portion of the tube within the tubesheet decreases the tubesheet displacement because it stiffens the tubesheet with respect to the bending caused by the primary-to-secondary pressure differential (Reference 3-7).

The upper five inches of the divider plate, stub runner and weld material is suppressed in the analysis of the combined thermal and pressure load cases to address concerns from the Nuclear Regulatory Commission regarding the potential for divider plate cracking. This condition is discussed in Reference 3-4, which details the assessment of a fully degraded divider plate to tubesheet weld in terms of the divider plate factors discussed in Reference 3-1 and 3-2. In the current analysis, a variant of the 3-D FEA lower tubesheet complex model was created that excluded the upper five inches of the divider plate and application of this model directly confirmed the conclusions of References 3-1 and 3-2 that this assumption is conservative relative to H*.

3.2.3 Input

The input for this analysis consists of steam generator dimensions for the plants to be analyzed, material properties from the ASME code, and pressure and temperature conditions from the PCWG parameters and transients.

The input boundary conditions for the limiting plants are Table 3-1 and Table 3-2 for the Model F plants and Model D5 plants, respectively. The modulus of elasticity and coefficients of thermal expansion are provided in Table 3-3 and Table 3-4. The tubesheet is SA-508 Class 2A, the divider plate is Alloy 600 (SB-168), the channelhead is SA-216 grade WCC, and the lower shell is SA-533 Grade A Class 2. These are the same values included in References 3-1 and 3-2.

3.2.4 Geometry

The geometry analyzed for the Model F and D5 SGs is essentially identical to that considered in the baseline analyses in References 3-1 and 3-2. The only modifications were the addition of several model partitions in the tubesheet region and truncating the divider plate. The first partition in the tubesheet model is at two inches from the secondary surface to accommodate a non-linear temperature profile. Additional solid body partitions were made through the tubesheet at distances equal to one and two pitches behind the half-symmetry plane to facilitate the post-processing of displacements for the square cell model. The typical solid models used are shown in Figure 3-1 for the Model F SGs (Millstone 3) showing the truncated divider plate and Figure 3-2 for the Model D5 SG (Byron/Braidwood 2) showing the model with the complete divider plate.

For the current H* analysis, the upper five inches of the divider plate, stub runner and weld material is suppressed in the analysis of the combined thermal and pressure load cases. This approach, used to avoid potential concerns regarding cracking of the divider plate was shown in prior analysis to be conservative for H* References 3-1 and 3-2, Section 6.2.6. Figure 3-1 shows a typical representation of the solid body with the upper five inches of the divider plate and attached materials suppressed. Eliminating this material in the model does not change the application or values of the applied boundary conditions nor does it change the results of the thermal analysis. The only effect that truncating the divider plate has is that the tubesheet has less resistance to the applied pressure loads than if it were connected to the divider plate.

However, the steam generator model with the severed divider plate is the same model as the steam generator with an intact divider plate in all other respects.

3.2.5 Mesh Discussion

The meshes used in this analysis are similar to the fine mesh used in the baseline analyses in References 3-1 and 3-2. Additional constraints were added in order to accommodate the vertical partition through the tubesheet. The mesh used in the analysis is similar to the one used in the baseline analysis described in References 3-1 and 3-2. The mesh for Millstone Unit 3 is shown in Figure 3-3, Figure 3-4, and Figure 3-5 for the principal axes. The meshing scheme for other model SGs is similar to that shown in Figures 3-3 through 3-5.

The model meshes used in the analyses for the Model D5 and Model F SGs are essentially the same as the fine mesh used in the reference analyses in References 3-1 and 3-2. Additional constraints were added to the current mesh to accommodate the vertical partition through the tubesheet. The mesh for the Model F (Millstone 3) model is shown in Figure 3-3, Figure 3-4, and Figure 3-5 for the principal axes. The model meshes for other model SGs are similar but accommodate the specific geometry of the other Models of SGs.

3.2.6 Tubesheet Equivalent Properties

Modeling of the equivalent properties of the perforated plate (tubesheet) by the method of Slot is discussed in Section 6.2.1 of References 3-1 and 3-2. The same equivalent properties used in References 3-1 and 3-2 were used in the current analysis. Information from those references is included here for completeness. Interpolated ratios of equivalent properties are in Table 3-5, where the "*" indicates the properties of the equivalent tubesheet. The ratios are then multiplied by the material properties for SA-508 Class 2A in Table 3-3 to obtain the temperature-dependent equivalent properties. The equivalent properties for the tubesheet are in Table 3-6 and Table 3-7 for the Model F SG and Model D5 SG, respectively.

3.2.7 Boundary Conditions

The application of the boundary conditions to the models is consistent with those included in the current licensing basis, Reference 3-1 and Reference 3-2. Table 3-1 and 3-2 summarize the specific boundary conditions and how they are applied to the 3-D-FEA model. Two different analyses were performed with the 3-D FEA model of the lower SG tubesheet complex to support application of the C^2 model:

1. Thermal Analysis: The operating temperature conditions only were applied to the SG, with a reference temperature of 70°F. The result from this analysis is purely a temperature profile through the tubesheet.

2. Deflection Analysis: In this analysis, the non-uniform temperature profile from the first analysis and the pressure loads are simultaneously applied to the model. The results from this analysis, with the severed divider plate condition, are used in the final H* analysis. Instead of accounting for the absence of the divider plate by application of a divider plate

factor, as in the licensing basis analysis. All of the required displacements and effects are directly accounted for by ANSYS.

The results of the second analysis provide the input for subsequent analysis with the square cell model which replaces the thick shell model in the current licensing basis. The approach in the second analysis is beneficial because it eliminates the need to separately post-process and calculate the different displacements required for the H* analysis, as was done in the licensing basis.

The applied loads and temperatures in each analysis are shown in Table 3-1 and Table 3-2. The analysis was applied only to the limiting conditions required for H*; that is, if a plant's limiting H* distance is controlled by the normal operating (NOP) condition, the NOP pressures and temperature loads were used in the analysis and the SLB conditions were not considered and vice versa.

3.2.8 Tubesheet Complex 3-D FEA Analysis Results

Figure 3-6 shows the results of the thermal analysis for Millstone for normal operating conditions. The thermal profile is slightly different than that in the licensing basis document, but is more accurate due to the direct application of temperature loads to the tubesheet partition. Figures 3-7 through 3-9 show the results of the thermal-structural analysis for Millstone for 100% power. Figure 3-10 shows the results of the SLB thermal analysis for Millstone. Aside from the severed divider plate, these results are the same as in the licensing basis. Figures 3-11 and 3-12 show the X- and Z-deformations for SLB for Millstone Unit 3. The results of the current 3-D FEA as documented in this report are taken from Reference 3-6.

Table 3-1 Input Boundary Conditions for Model F (Millstone Unit 3)

Parameter	Low T_{avg}	SLB
Hot Leg Pressure (psia)		
SG Outlet Pressure (psia)		
Secondary Pressure (psia)		
Hot Leg Temperature (°F)		
SG Outlet Temperature (°F)		
Steam Temperature (°F)		
Feedwater Temperature (°F)		
Mean Shell Radius r_m (inches)		
Shell Thickness t (inches)		
Calculated Values		
Secondary Fluid Temperature		
Endcap Load (psia)		

a,c,e

Table 3-2 Input Boundary Conditions for Model D5 (Byron/Braidwood Units 2)

Parameter	Low T_{avg}	SLB
Hot Leg Pressure (psia)		
SG Outlet Pressure (psia)		
Secondary Pressure (psia)		
Hot Leg Temperature (°F)		
SG Outlet Temperature (°F)		
Steam Temperature (°F)		
Feedwater Temperature (°F)		
Mean Shell Radius r_m (inches)		
Shell Thickness t (inches)		
Calculated Values		
Secondary Fluid Temperature		
End cap Load (psia)		

a,c,e

Table 3-3 Modulus of Elasticity for Materials

Temperature (°F)	SA-508 Class 2A (Msi)	Alloy 600 (Msi)	SA-216 Grade WCC (Msi)	SA-533 Grade A Class 2 (Msi)
70	29.2	31.0	29.5	29.2
200	28.5	30.2	28.8	28.5
300	28.0	29.9	28.3	28.0
400	27.4	29.5	27.7	27.4
500	27.0	29.0	27.3	27.0
600	26.4	28.7	26.7	26.4
700	25.3	28.2	25.5	25.3

Table 3-4 Coefficient of Thermal Expansion for Materials

Temperature (°F)	SA-508 Class 2A (µin/in)	Alloy 600 (µin/in)	SA-216 Grade WCC (µin/in)	SA-533 Grade A Class 2 (µin/in)
70	6.50	6.90	5.53	7.06
200	6.67	7.20	5.89	7.25
300	6.87	7.40	6.26	7.43
400	7.07	7.57	6.61	7.58
500	7.25	7.70	6.91	7.70
600	7.42	7.82	7.17	7.83
700	7.59	7.94	7.41	7.94

Table 3-5 Interpolated Ratios of Equivalent Material Properties for Analysis of Perforated Plate

Property	Model F[(1)]	Model D5
Gy*/ Gy	[	]
Ey*/ Ey	[	]
Ep*/ Ep	[	]
Gp*/Gp	[	]
Poisson's Ratio	[	]

a,c,e

Notes:

(1) These values differ from the values shown in Reference 3-1; however, they are the correct values used in the analysis documented in Reference 3-1.

Table 3-6 Equivalent Properties for Tubesheet for Model F SG (Millstone 3)

Temperature	Out-of-Plane		In-Plane	
(°F)	E (Msi)	G (Msi)	E (Msi)	G (Msi)
70				
200				
300				
400				
500				
600				
700				

a,c,e

Table 3-7 Equivalent Properties for Tubesheet for Model D5 SG (Byron / Braidwood Unit 2)

Temperature	Out-of-Plane		In-Plane	
(°F)	E (Msi)	G (Msi)	E (Msi)	G (Msi)
70				
200				
300				
400				
500				
600				
700				

a,c,e

Figure 3-1 Typical Representation of Severed Divider Plate Condition; Model F (Millstone 3 configuration shown)

Figure 3-2 Typical Solid Model for Intact Divider Plate; Model D5 (Byron/Braidwood Unit 2 configuration shown)

a,c,e

Figure 3-3 Model F (Millstone 3) Mesh, View down Z-axis

a,c,e

Figure 3-4 Model F (Millstone 3) Mesh, View down Y-Axis

a,c,e

Figure 3-5 Model F (Millstone 3) Mesh, View down X-Axis

a,c,e

Figure 3-6 Model F (Millstone 3) Results of NOP Thermal Analysis

Figure 3-7 Model F (Millstone 3) Results of Thermal-Structural Analysis, Y Deformation

Figure 3-8 Model F (Millstone 3) Results of Thermal-Structural Analysis, X Deformation on Hot Leg Face

a,c,e

Figure 3-9 Model F (Millstone 3) Results of Thermal-Structural Analysis, Z Deformation on Hot Leg

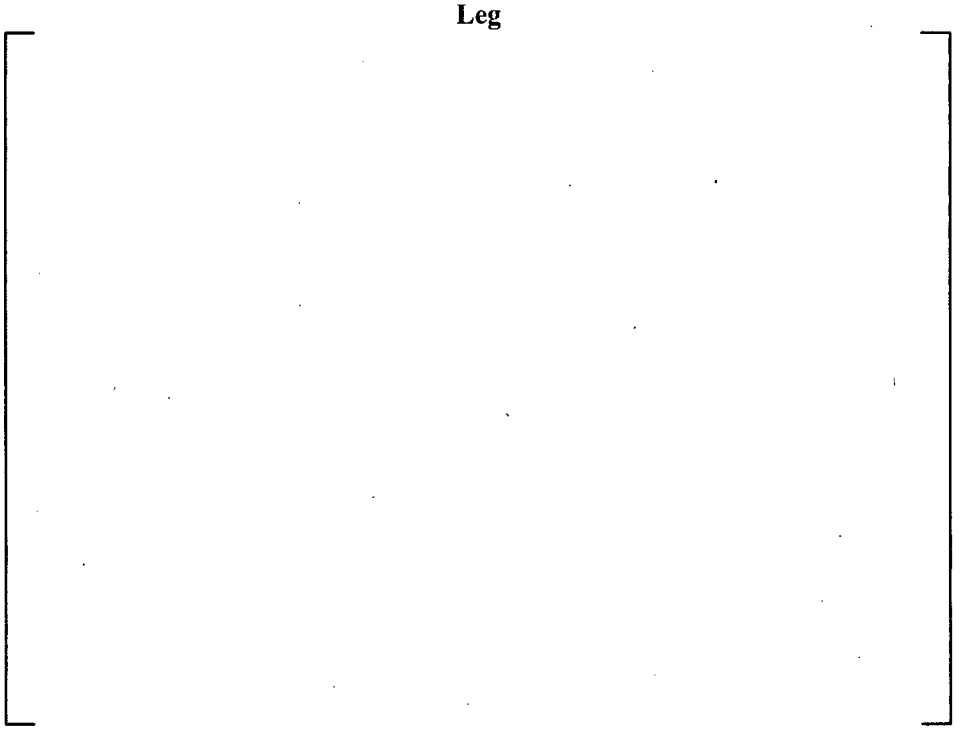

a,c,e

Figure 3-10 Model F (Millstone 3) Results of SLB Thermal Analysis


a,c,e

Figure 3-11 Model F (Millstone 3) Results of SLB Thermal-Structural Analysis, X Deformation on Hot Leg Face

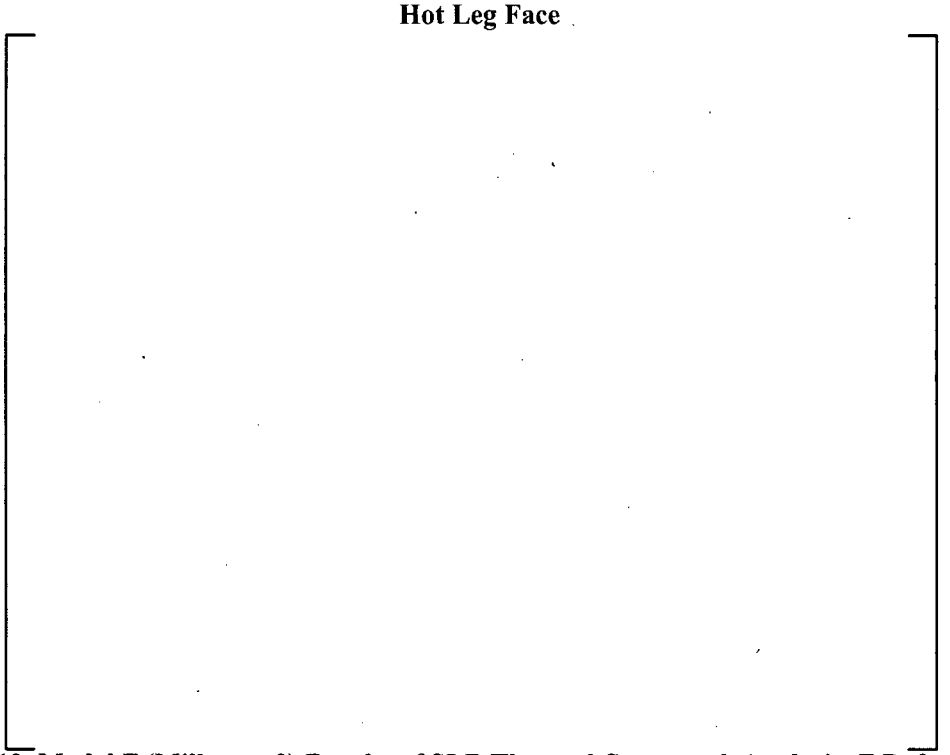
a,c,e

Figure 3-12 Model F (Millstone 3) Results of SLB Thermal-Structural Analysis, Z Deformation on Hot Leg

3.3 CALCULATION OF MEAN H* FROM C^2 MODEL

3.3.1 Method Discussion

The structural finite element analysis is based on a 2-D pseudo sub-model of the SG tubesheet and corresponding tube throughout the entire tubesheet thickness of approximately 21 inches. This model is then quartered to simplify the computations as seen in Figure 3-13.

Each tubesheet radius of each SG model is computed and graphed separately. At each tubesheet radius, there are nine elevations at which the contact pressure is calculated. For each operating condition, a thermal and thermal-structural analysis was performed with the 3-D FEA model (see Sections 3.1 and 3.2) to determine the tubesheet displacements used as input to the square cell model to calculate the contact pressures of the tubes with regards to the tubesheet. All of the analyses were static and linear elastic.

a,c,e

Figure 3-13 Sub-Model for Computational Analysis

3.3.2 Development of Displacements for Square Cell

The displacements to apply to the square cell model are calculated from the displacements on the 3-D model using a finite difference technique to approximate the strain. The applied displacements simulate the strain across one-half of one pitch of the steam generator from all of the loads applied to the 3-D FEA model. There are two displacements to consider, those in the X-direction and those in the Z-direction (both in the same plane). For calculation of the displacements in the X-direction, the X-displacements on the hot leg face of the perforated section of the tubesheet are utilized. After being exported from ANSYS, they are processed using a finite difference method to calculate the strain, which is the derivative of displacement. This utilizes the central difference formula of second order (Reference 3-5, pp 83-85):

$$\varepsilon_i = \frac{\partial U_{x,i}}{\partial x} \approx \frac{U_{x,i+1} - U_{x,i-1}}{2\Delta x} \qquad \text{(Equation 3-1)}$$

At the edges of the perforated region, of necessity, the forward and backward differences of second order are used:

$$\varepsilon_i = \frac{\partial U_{x,i}}{\partial x} \approx \frac{-U_{x,i+2} + 4U_{x,i+1} - 3U_{x,i}}{2\Delta x}$$
$$\varepsilon_i = \frac{\partial U_{x,i}}{\partial x} \approx \frac{+U_{x,i-2} - 4U_{x,i-1} + 3U_{x,i}}{2\Delta x}$$

(Equation 3-2)

The displacement to apply to the square cell model is the strain times the length of the model, which is one-half of a pitch:

$$\Delta x_{squarecell} = 0.5 * P * \varepsilon_x$$

(Equation 3-3)

The calculation of the z displacements uses the z-displacements from the 3-D FEA model which are two pitches back from the hot leg face. A similar central difference formula is used to calculate the derivative:

$$\varepsilon_i = \frac{\partial U_{z,i}}{\partial z} \approx \frac{U_{z,i+2} - U_{z,i}}{2\Delta z}$$

(Equation 3-4)

This equation is slightly modified to calculate the strain in the z direction one pitch back from the cut face of the 3-D model. This is necessary because the cut face has a symmetry condition in the z-direction; therefore, the strain in the z direction necessarily vanishes there. Since the displacement is zero on that face, the equation can be simplified:

$$\varepsilon_i = \frac{\partial U_{z,i}}{\partial z} \approx \frac{U_{z,i+2}}{2P}$$

(Equation 3-5)

Calculation of the applied displacements from the strain is identical:

$$\Delta z_{squarecell} = 0.5 * P * \varepsilon_z$$

(Equation 3-6)

3.3.3 Discussion of Significant Assumptions

The axial thermal profile for the tubesheet is discussed in Section 3.2. In the thermal analysis, the secondary side of the tubesheet was assumed to be at a temperature equal to the average of the steam temperature and the feedwater temperature.

The dimensions used for the finite element model were consistent with the current licensing basis.

The divider plate was assumed to have the top five inches removed to account for a potentially degraded tubesheet to divider plate weld as discussed in Section 3.2.

The current results exclude any residual contact pressure effects from the tube hydraulic expansion.

In terms of the connections between the tube and tubesheet, this model uses a friction coefficient of [ ]^{a,c,e} (Reference 3-2), and a pinball radius of [ ]^{a,c,e} inches, which is half the value of the surface roughness tolerance from Reference 3-15. The pinball radius is the tolerance within which contact at a node is assumed by the structural code. The analysis also uses a normal stiffness factor of [ ]^{a,c,e}, which dictates how quickly the model will converge depending on the degree of bending deformation, which was based on several trials that defined this value for acceptable convergence of the model.

Concerning the tube bending in the tubesheet, the square cell model does not use the Goodier model to assume the tubesheet collar is a continuous structure. The applied loading on the tubesheet bends the tube. This bending is caused by temperature change as well as the pressure differential across the tubesheet and increases contact pressure. Neglecting tubesheet bending is conservative because the increased contact pressure between the tube and the tubesheet would reduce the H* distance.

3.3.4 Input

The input for this analysis consists of steam generator dimensions for the plants to be analyzed, material properties from the ASME code, and pressure and temperature conditions from the PCWG parameters and transients. The dimensions, the material properties, the PCWG parameters used for the D5 and F models, the input for the Model Fs and the input for the Model D5s are taken from Reference 3-1 and 3-2, respectively.

Because the analysis is a static, linear, elastic methodology, the material properties used as inputs are the elastic moduli and coefficients of thermal expansion. The tubesheet is SA-508 Class 2A and the tube is Alloy 600 Thermally Treated (TT). The modulus of elasticity and coefficients of thermal expansion are taken from References 3-1 and 3-2.

3.3.5 Geometry

Figure 3-14 shows a representation of the solid model used. The model was created in ANSYS Workbench Design Modeler. The associated representative dimensions for all models are shown in Figure 3-15.

3.3.6 Mesh

The mesh used in the analysis combines the tube and tubesheet in one model and creates one mesh for both pieces. This mesh is based on work done in Section 2.5.2. This grid of nodes allows for easy post-processing and interpolation of deformations on the face. The density in this region is judged to be adequate from experience and comparison to prior models (i.e., Reference 3-6). The actual mesh for all models analyzed is shown in Figure 3-16.

a,c,e

Figure 3-14 Representative Solid Model

a,c,e

Figure 3-15 Representative Dimensions for All Models

a,c,e

Figure 3-16 Implemented Model Mesh, View Down Z-Axis

3.3.7 Boundary Conditions

The applied boundary conditions consisted of pressure loads, thermal loads, and constraints. The pressure loads consisted of the crevice pressure, the pressure difference inside the tube. The thermal loads were applied as fixed temperature boundary conditions on the bodies for the thermal analysis. Three constraints applied.

1. The upper edge of the model was constrained in the X-direction.

2. The lower edge of the model was constrained in the Y-direction.

3. The pressure differential on the tube was determined as the difference between the primary pressure on the tube ID and the crevice pressure on the tube OD.

The application of these boundary conditions is shown in Figure 3-17.

All of the applied loads and temperatures are described in Section 3.2.

(Note: For analytical convenience, the coordinate system for this model is X-Y, which is equivalent to the X-Z SG coordinates as noted in Section 2.)

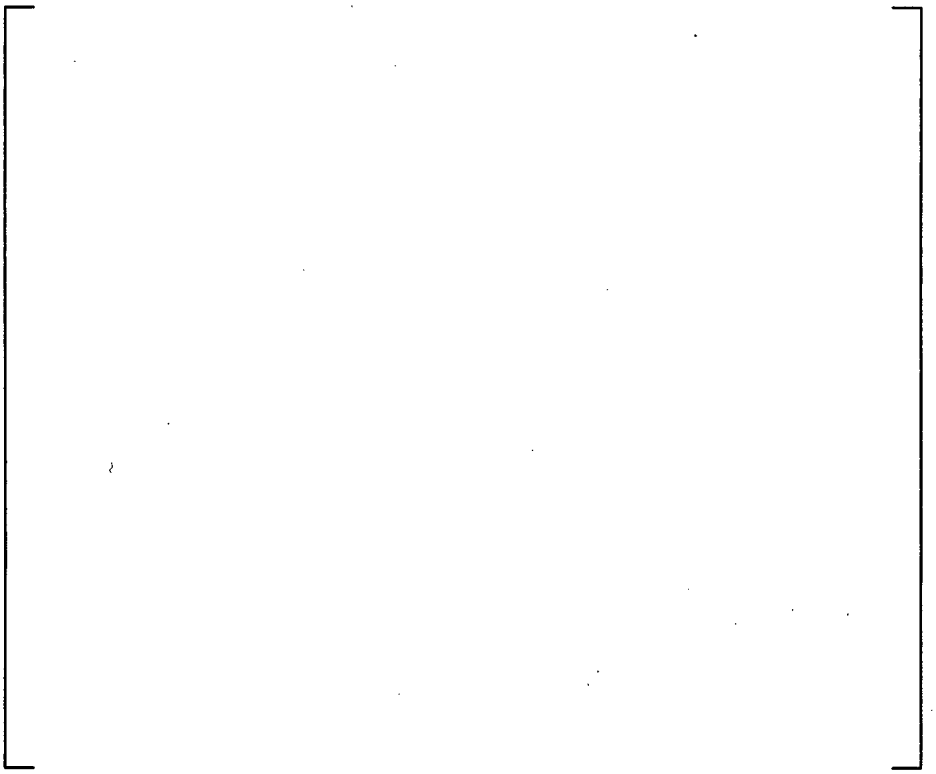

a,c,e

Figure 3-17 Boundary Conditions for All Models

3.3.8 C^2 FEA Results

Inputs and contact pressure plots of the finite element analysis (FEA) results for each individual model, radius and elevation are included in this section. The thermal analysis results are steady-state with fixed boundary conditions as documented in Reference 3-8.

Within each table, the explanations of the categories are as follows: TS Elevation stands for tubesheet elevation, delta X and delta Z represent the displacement in the respective direction of the square cell model, delta P represents the difference between the reference pressure and the crevice pressure which was empirically determined, temperature is self explanatory, and P_{con} Theta represents the contact pressure between the tube and tubesheet.

3.3.9 Model D5 (Byron/Braidwood 2) FEA Results

The spreadsheet results of the Model D5 FEA analysis are in Tables 3-8 through 3-13. These results are used to produce the graphical results for each tubesheet radius in Figures 3-18 to 3-23. Tables are provided for each of the NOP, SLB, and FLB conditions in this section; the FLB condition figures appear in Section 4.0 to support the leakage assessment.

3.3.10 Model F (Millstone 3) FEA Results

The spreadsheet results of the Model F FEA analysis are in Table 3-14 through 3-19. These results are used to produce the graphical results for each radius in Figures 3-24 to 3-29. Tables are provided for the NOP and SLB conditions. A qualitative assessment of the factors that influence contact pressure was performed which shows that contact pressures for FLB conditions would exceed those in the current licensing basis, and thus, explicit analysis is unnecessary (Reference 3-16).

3.3.11 Model D5 Contact Pressure Profiles

The results of the FEA analysis for the Model D5 that were calculated in Section 3.3.9 are shown below in Figure 3-18 through 3-23. These figures show the contact pressure trends between the normal operating condition versus the steam line break conditions at various elevations between 0.0 and 21.030 inches, where 0.0 represents the top of the tubesheet and 21.030 represents the bottom of the tubesheet.

3.3.12 Model F Contact Pressure Profiles

The results of the FEA analysis for the Model F that were calculated in Section 3.3.10 are shown below in Figures 3-24 through 3-29. These figures show the contact pressure trends between the normal operating condition versus the steam line break conditions at various elevations between 0.0 and 21.030 inches, where 0.0 represents the top of the tubesheet and 21.030 represents the bottom of the tubesheet.

Table 3-8 Model D5 Byron/Braidwood Inputs and Results, 4.437 in Radius

NOP						
	TS Elevation	ΔX	ΔZ	ΔP	Temperature	Pcon Theta
	in	in	in	psi	°F	psi
BTS	0.000	[				] a,c,e
	2.000					
	4.000					
	6.000					
NA	10.515					
	16.901					
	19.030					
	20.030					
TTS	21.030					

SLB						
	TS Elevation	ΔX	ΔZ	ΔP	Temperature	Pcon Theta
	in	in	in	psi	°F	psi
BTS	0.000	[				] a,c,e
	2.000					
	4.000					
	6.000					
NA	10.515					
	16.901					
	19.030					
	20.030					
TTS	21.030					

FLB						
	TS Elevation	ΔX	ΔZ	ΔP	Temperature	Pcon Theta
	in	in	in	psi	°F	psi
BTS	0.000	[				] a,c,e
	2.000					
	4.000					
	6.000					
NA	10.515					
	16.901					
	19.030					
	20.030					
TTS	21.030					

Table 3-9 Model D5 Byron/Braidwood Inputs and Results, 10.431 in Radius

NOP						
	TS Elevation	ΔX	ΔZ	ΔP	Temperature	Pcon Theta
	in	in	in	psi	°F	psi
BTS	0.000	[				] a,c,e
	2.000					
	4.000					
	6.000					
NA	10.515					
	16.901					
	19.030					
	20.030					
TTS	21.030					

SLB						
	TS Elevation	ΔX	ΔZ	ΔP	Temperature	Pcon Theta
	in	in	in	psi	°F	psi
BTS	0.000	[				] a,c,e
	2.000					
	4.000					
	6.000					
NA	10.515					
	16.901					
	19.030					
	20.030					
TTS	21.030					

FLB						
	TS Elevation	ΔX	ΔZ	ΔP	Temperature	Pcon Theta
	in	in	in	psi	°F	psi
BTS	0.000	[				] a,c,e
	2.000					
	4.000					
	6.000					
NA	10.515					
	16.901					
	19.030					
	20.030					
TTS	21.030					

Table 3-10 Model D5 Byron/Braidwood Inputs and Results, 18.139 in Radius

NOP						
	TS Elevation	ΔX	ΔZ	ΔP	Temperature	Pcon Theta
	in	in	in	psi	°F	psi
BTS	0.000	[				] a,c,e
	2.000					
	4.000					
	6.000					
NA	10.515					
	16.901					
	19.030					
	20.030					
TTS	21.030					

SLB						
	TS Elevation	ΔX	ΔZ	ΔP	Temperature	Pcon Theta
	in	in	in	psi	°F	psi
BTS	0.000	[				] a,c,e
	2.000					
	4.000					
	6.000					
NA	10.515					
	16.901					
	19.030					
	20.030					
TTS	21.030					

FLB						
	TS Elevation	ΔX	ΔZ	ΔP	Temperature	Pcon Theta
	in	in	in	psi	°F	psi
BTS	0.000	[				] a,c,e
	2.000					
	4.000					
	6.000					
NA	10.515					
	16.901					
	19.030					
	20.030					
TTS	21.030					

Table 3-11 Model D5 Byron/Braidwood Inputs and Results, 26.703 in Radius

NOP						
	TS Elevation	ΔX	ΔZ	ΔP	Temperature	Pcon Theta
	in	in	in	psi	°F	psi
BTS	0.000					
	2.000					
	4.000					
	6.000					
NA	10.515					
	16.901					
	19.030					
	20.030					
TTS	21.030					

a,c,e

SLB						
	TS Elevation	ΔX	ΔZ	ΔP	Temperature	Pcon Theta
	in	in	in	psi	°F	psi
BTS	0.000					
	2.000					
	4.000					
	6.000					
NA	10.515					
	16.901					
	19.030					
	20.030					
TTS	21.030					

a,c,e

FLB						
	TS Elevation	ΔX	ΔZ	ΔP	Temperature	Pcon Theta
	in	in	in	psi	°F	psi
BTS	0.000					
	2.000					
	4.000					
	6.000					
NA	10.515					
	16.901					
	19.030					
	20.030					
TTS	21.030					

a,c,e

Table 3-12 Model D5 Byron/Braidwood Inputs and Results, 42.974 in Radius

NOP							
	TS Elevation	ΔX	ΔZ	ΔP	Temperature	Pcon Theta	
	in	in	in	psi	°F	psi	
BTS	0.000	[					a,c,e
	2.000						
	4.000						
	6.000						
NA	10.515						
	16.901						
	19.030						
	20.030						
TTS	21.030					]	

SLB							
	TS Elevation	ΔX	ΔZ	ΔP	Temperature	Pcon Theta	
	in	in	in	psi	°F	psi	
BTS	0.000	[					a,c,e
	2.000						
	4.000						
	6.000						
NA	10.515						
	16.901						
	19.030						
	20.030						
TTS	21.030					]	

FLB							
	TS Elevation	ΔX	ΔZ	ΔP	Temperature	Pcon Theta	
	in	in	in	psi	°F	psi	
BTS	0.000	[					a,c,e
	2.000						
	4.000						
	6.000						
NA	10.515						
	16.901						
	19.030						
	20.030						
TTS	21.030					]	

Table 3-13 Model D5 Byron/Braidwood Inputs and Results, 49.825 in Radius

NOP						
	TS Elevation	ΔX	ΔZ	ΔP	Temperature	Pcon Theta
	in	in	in	psi	°F	psi
BTS	0.000					
	2.000					
	4.000					
	6.000					
NA	10.515					
	16.901					
	19.030					
	20.030					
TTS	21.030					

a,c,e

SLB						
	TS Elevation	ΔX	ΔZ	ΔP	Temperature	Pcon Theta
	in	in	in	psi	°F	psi
BTS	0.000					
	2.000					
	4.000					
	6.000					
NA	10.515					
	16.901					
	19.030					
	20.030					
TTS	21.030					

a,c,e

FLB						
	TS Elevation	ΔX	ΔZ	ΔP	Temperature	Pcon Theta
	in	in	in	psi	°F	psi
BTS	0.000					
	2.000					
	4.000					
	6.000					
NA	10.515					
	16.901					
	19.030					
	20.030					
TTS	21.030					

a,c,e

Table 3-14 Model F Millstone Inputs and Results, 4.016 in Radius

NOP						
	TS Elevation	ΔX	ΔZ	ΔP	Temperature	Pcon Theta
	in	in	in	psi	°F	psi
BTS	0.000	[				] a,c,e
	2.000					
	4.000					
	6.000					
NA	10.515					
	16.901					
	19.030					
	20.030					
TTS	21.030					

SLB						
	TS Elevation	ΔX	ΔZ	ΔP	Temperature	Pcon Theta
	in	in	in	psi	°F	psi
BTS	0.000	[				] a,c,e
	2.000					
	4.000					
	6.000					
NA	10.515					
	16.901					
	19.030					
	20.030					
TTS	21.030					

Table 3-15 Model F Millstone Inputs and Results, 11.722 in Radius

NOP							
	TS Elevation	ΔX	ΔZ	ΔP	Temperature	Pcon Theta	
	in	in	in	psi	°F	psi	
BTS	0.000	[				]	a,c,e
	2.000						
	4.000						
	6.000						
NA	10.515						
	16.901						
	19.030						
	20.030						
TTS	21.030						

SLB							
	TS Elevation	ΔX	ΔZ	ΔP	Temperature	Pcon Theta	
	in	in	in	psi	°F	psi	
BTS	0.000	[				]	a,c,e
	2.000						
	4.000						
	6.000						
NA	10.515						
	16.901						
	19.030						
	20.030						
TTS	21.030						

Table 3-16 Model F Millstone Inputs and Results, 20.498 in Radius

NOP						
	TS Elevation	ΔX	ΔZ	ΔP	Temperature	Pcon Theta
	in	in	in	psi	°F	psi
BTS	0.000					
	2.000					
	4.000					
	6.000					
NA	10.515					
	16.901					
	19.030					
	20.030					
TTS	21.030					

a,c,e

SLB						
	TS Elevation	ΔX	ΔZ	ΔP	Temperature	Pcon Theta
	in	in	in	psi	°F	psi
BTS	0.000					
	2.000					
	4.000					
	6.000					
NA	10.515					
	16.901					
	19.030					
	20.030					
TTS	21.030					

a,c,e

Table 3-17 Model F Millstone Inputs and Results, 30.193 in Radius

NOP						
	TS Elevation	ΔX	ΔZ	ΔP	Temperature	Pcon Theta
	in	in	in	psi	°F	psi
BTS	0.000					
	2.000					
	4.000					
	6.000					
NA	10.515					
	16.901					
	19.030					
	20.030					
TTS	21.030					

a,c,e

SLB						
	TS Elevation	ΔX	ΔZ	ΔP	Temperature	Pcon Theta
	in	in	in	psi	°F	psi
BTS	0.000					
	2.000					
	4.000					
	6.000					
NA	10.515					
	16.901					
	19.030					
	20.030					
TTS	21.030					

a,c,e

Table 3-18 Model F Millstone Inputs and Results, 48.613 in Radius

NOP						
	TS Elevation	ΔX	ΔZ	ΔP	Temperature	Pcon Theta
	in	in	in	psi	°F	psi
BTS	0.000	[				] a,c,e
	2.000					
	4.000					
	6.000					
NA	10.515					
	16.901					
	19.030					
	20.030					
TTS	21.030					

SLB						
	TS Elevation	ΔX	ΔZ	ΔP	Temperature	Pcon Theta
	in	in	in	psi	°F	psi
BTS	0.000	[				] a,c,e
	2.000					
	4.000					
	6.000					
NA	10.515					
	16.901					
	19.030					
	20.030					
TTS	21.030					

Table 3-19 Model F Millstone Inputs and Results, 58.308 in Radius

NOP							
	TS Elevation	ΔX	ΔZ	ΔP	Temperature	Pcon Theta	
	in	in	in	psi	°F	psi	
BTS	0.000						a,c,e
	2.000						
	4.000						
	6.000						
NA	10.515						
	16.901						
	19.030						
	20.030						
TTS	21.030						

SLB							
	TS Elevation	ΔX	ΔZ	ΔP	Temperature	Pcon Theta	
	in	in	in	psi	°F	psi	
BTS	0.000						a,c,e
	2.000						
	4.000						
	6.000						
NA	10.515						
	16.901						
	19.030						
	20.030						
TTS	21.030						


a,c,e

Figure 3-18 Model D5 Contact Pressure Results, 4.437 in Radius

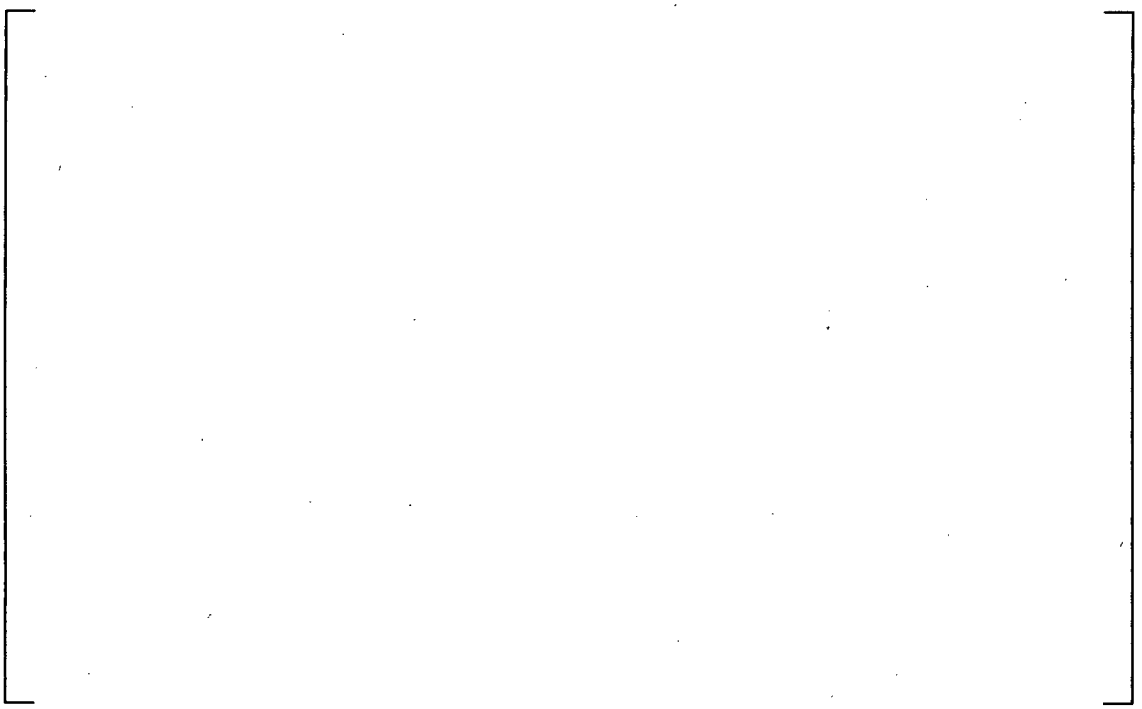
a,c,e

Figure 3-19 Model D5 Contact Pressure Results, 10.431 in Radius

0-TS Elevation is the Top of the Tubesheet

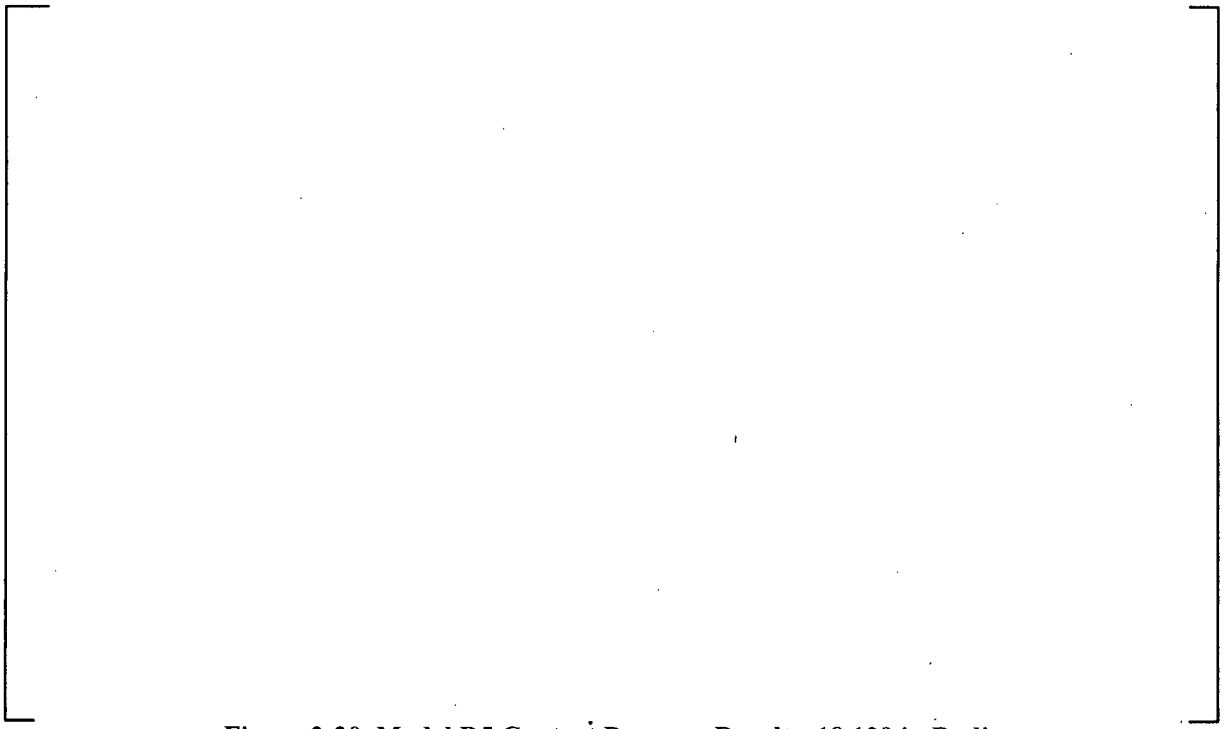

a,c,e

Figure 3-20 Model D5 Contact Pressure Results, 18.139 in Radius

a,c,e

Figure 3-21 Model D5 Contact Pressure Results, 26.703 in Radius

0-TS Elevation is the Top of the Tubesheet

a,c,e

Figure 3-22 Model D5 Contact Pressure Results, 42.974 in Radius

a,c,e

Figure 3-23 Model D5 Contact Pressure Results, 49.825 in Radius

0-TS Elevation is the Top of the Tubesheet

a,c,e

Figure 3-24 Model F Contact Pressure Results, 4.016 in Radius

a,c,e

Figure 3-25 Model F Contact Pressure Results, 11.722 in Radius

0-TS Elevation is the Top of the Tubesheet

a,c,e

Figure 3-26 Model F Contact Pressure Results, 20.498 in Radius

a,c,e

Figure 3-27 Model F Contact Pressure Results, 30.193 in Radius

0-TS Elevation is the Top of the Tubesheet

a,c,e

Figure 3-28 Model F Contact Pressure Results, 48.613 in Radius

a,c,e

Figure 3-29 Model F Contact Pressure Results, 58.308 in Radius

0-TS Elevation is the Top of the Tubesheet

3.3.13 Mean H* Calculations

Once the contact pressures were calculated for each radius of each model, it is then possible to calculate a mean H* for each radius of each model.. The equation used is the same as in Reference 3-1 and 3-2, Equation 1-3. Table 3-20 contains the inputs used to determine the H*'s along with the contact pressures.

Equation 1-3 from References 3-1 and 3-2 generates the accumulated pull out load throughout the thickness of the tubesheet at each elevation. These accumulated pull out loads are then integrated using the trapezoidal rule along with the predetermined pull out loads for each model (References 3-1 and 3-2) to generate the mean H* for that radius. Table 3-21 shows the results of these calculations for each radius of each mode. From these values, the critical radius is determined by the largest value for each model.

Table 3-20 H* Input Summary

(References 3-1 and 3-2)

	NOP	SLB
SG Model/Tube OD	**End cap Load (lb)**	**End cap Load (lb)**
D5/[0.762][a,c,e]	[	] a,c,e
F/[0.7608][a,c,e]	[	]
End cap loads based on 3ΔP for H* structural analysis		

Table 3-21 Summary of H* Mean Values

(all dimensions in inches)

SG Model	Radius	NOP H*	SLB H*
F	4.016	[a,c,e	(1)
	11.722		
	20.498		
	30.193		
	48.613		
	58.308	]	
D5	4.437	(2)	[a,c,e
	10.431		
	18.139		
	26.703		
	42.974		
	49.825		]
Notes: (1) The limiting condition for the Model F SG is NOP. (2) The limiting condition for the Model D5 SG is SLB.			

3.4 CALCULATION OF PROBABILISTIC H* USING THE C^2 MODEL

This section provides a comparison between the square cell (C^2) structural model and the licensing basis structural model in terms of the probabilistic evaluation of H*. The Monte-Carlo simulation process by which the distribution of H* is computed for a given CTE response surface is described in Reference 3-14. The analyses described in this section investigate the relative behavior of the square cell and licensing basis models in the local region of CTE space (tube-CTE, tubesheet-CTE) determined in the current licensing basis to include the 95th percentile value of H*. Guidance for the methods discussed in this section was taken from Reference 3-10.

The square cell (C^2) analysis is an independent method of modeling the contact pressure distribution between the tube and the tubesheet used to calculate H*. The results can be compared to those of the licensing basis for the permanent H* ARC. The results of using the square cell analysis show that the mean value of H* and the probabilistic estimate of the H* value at the required probability level change compared to the existing licensing basis values. The Model D5 SG probabilistic H* value decreases by 3.59 inches and the Model F SG probabilistic value increases by 2.1 inches. These changes to the current licensing basis values are caused by the calculation of updated tubesheet displacements and contact pressures than were documented in References 3-1 and 3-2 and discussed above in Sect 3.2 and 3.3 of this report.

3.4.1 Assumptions

The assumptions made for the structural analyses of the tubes and tubesheet also apply to the analysis of the probabilistic value of H*. Sections 3.1 through 3.3 of this report provide a detailed description of those assumptions. Additional assumptions and observations that apply only to the probabilistic H* and Monte Carlo (MC) analysis are:

1. The critical region of the H* response surface will remain at a combination of decreasing tube CTE (- $n\sigma_T$) and increasing tubesheet CTE (+$n\sigma_T$). This assumption was previously shown to maximize the value of H*. At large variations from the mean, the tubesheet will grow away from the tube and there will be zero contact pressure contribution from thermal effects ("lock-up"). Variations of Young's modulus has been shown to have negligible effect on H* in prior analyses.

2. Both the C^2 model and the thick shell model represent the similar physical structure; thus, both models are expected to yield the same trend in their response to variations of material properties.

3. In the range of interest (e.g., above the 90th percentile), the H* rank order statistic results from a series of material property combinations, predicted by a full bundle Monte Carlo simulation with 10,000 trials, will remain essentially linear regardless of which structural model is applied. This assumption is shown to be true in the subsequent analysis.

4. The sensitivity of the square cell model contact pressure results to adjusting the tube length based on the crevice pressure distribution is similar to the curves developed for the H* analysis in References 3-1 and 3-2. (Note that a new crevice pressure distribution adjustment curve for the SLB condition in the Model D5 SG is provided in this section.)

3.4.2 Methods Discussion

The process for the probabilistic analysis based on the C^2 model is summarized in the following steps:

1. The structural response surface is determined in the current licensing basis, i.e., Figure 8-5 in the respective WCAP reports, References 3-1 and 3-2.

2. Based on the Monte Carlo evaluation using the specific response surfaces as documented in Reference 3-13, the values of the significant variables, the coefficients of thermal expansion of the tube and the tubesheet materials that lead to the required probabilistic values of H* (i.e., 95% probability at 50% confidence), can be determined.

3. Application of the combination of coefficients of thermal expansion determined in Step 2 to the C^2 model will yield the probabilistic values of H* based on the C^2 model. Because the inputs for the C^2 model are taken from the output of the 3-D FEA model, this involves also performing 3-D FEA model analyses using the tubesheet CTE values.

The method for developing the comparison response surface using the square cell analysis begins with the Monte Carlo analysis results from the licensing basis analysis. The results for the upper 10% tail of the H* distribution (e.g., rank order 9000 to rank order 10,000 in 10,000 simulations) from the licensing basis analysis were output as a four column by 1000 row vector. The values in the vector correspond to the rank order statistic, the H* value at a given rank order, the variation in the tubesheet CTE about its mean value in terms of nσ, and the variation in the tube CTE about its mean value in terms of nσ where nσ is the number and direction (positive or negative) of standard deviations added to the mean value of the respective CTEs (see for example Table 3-25). The mean values of CTEs for the tube and the tubesheet and their respective standard deviations ([ ]^{a,c,e}% for the tube material CTE and [ ]^{a,c,e}% for the tubesheet material) are taken from the licensing basis documentation, References 3-1 and 3-2.

The H* results from the licensing basis analysis include the effect of the tubesheet thermal distribution offset, and a 0.3 inch adder to address potential uncertainty in the location of the bottom of the expansion transition (BET) at the top of the tubesheet (TTS) but do not include the adjustment for crevice pressure or any benefit from the installation process (e.g., residual contact pressure). Section 6.4.5; Section 6.4.8 and Section 8.1.1 in Reference 3-1 discuss the effects of crevice pressure and the reasons for adjusting the final tube length in the H* calculation process. Figures 3-30 and 3-31 provide the crevice pressure distribution adjustment curves for the Model F and Model D5 SGs, respectively. The results of the licensing basis analysis were considered as a function of the combined uncertainties of the tube and tubesheet CTE vs. H*. It is possible to use the combined uncertainty approach because the limiting H* result occurs at a combination of tube and tubesheet properties with increasing (positive) tubesheet CTE variations and decreasing (negative) tube CTE variations. Because the combination of the tube and tubesheet properties that lead to the maximum value of H* always occur in the same quadrant, the sign of the material property variation is conserved and the region of the response surface to be compared is also conserved.

Reference 3-13 discusses the method for combining the significant variables for probabilistic analysis. Figure 3-32 shows the relation between the combined significant variables and the H* values above the 90th percentile from the licensing basis analysis for the Model D5 SG. The same general form of the data

occurs in each of the model SG considered when evaluated in this fashion. The lower bound of the data is termed the "break line." The break line is the maximum value of H* for a constant value of the combined significant variables affecting H*. Therefore, the break line contains the limiting H* for the specific SG model being considered. The "break line" can be fit by proper selection of the data points that define the lower bound of the data. Because the value of the combined significant variables are taken directly from the rank ordered results from the original analysis, the break line can also be defined in terms of the rank order instead of H* values. Figure 3-33 shows the break line defined by the rank order of the points selected.

The break line is used to determine specific values of the tube and tubesheet CTE to be used in a series of structural analysis cases using both the 3-D FEA model and the C^2 model. Note that the specific values of tubesheet CTE are always greater than the mean and the specific values of tube CTE are always less than the mean. The points selected are typically above and below the required probabilistic estimates (rank order) to produce a conservative result that bounds the needed value of H* without extrapolating data. The probabilistic estimates (defined as the rank order from 10,000 simulations) required for each of the limiting plants in the H* fleet are listed in Table 3-22. The points selected for each of the limiting plants in the H* fleet are listed in Table 3-23.

The selected values of the tubesheet CTE are used in a 3-D finite element analysis of the lower SG complex. The models, analysis method, assumptions and inputs to the lower SG complex analysis are the same to those described in References 3-1 and 3-2 but the model is modified to eliminate the upper five inches of the divider plate and re-meshed to provide the proper output displacement for the C^2 model. The resulting tubesheet displacements calculated from the model using the increased tubesheet CTE, with the matching decreased tube CTE properties, become inputs to the square cell model analysis as described in Section 2 of this report. The resulting contact pressures are then used to calculate the value of H* for that combination of tube and tubesheet CTE. This process is repeated for each of the selected data points along the break line. The H* values calculated using the new inputs to the square cell model correspond to the rank order statistic from the licensing basis.

The H* values for the same values of rank order statistic in the licensing basis and the square cell analysis are directly compared by plotting the resulting H* values as a function of the rank order statistic. See Figure 3-34 for the typical result based on the Model D5 SG NOP condition analysis. The data in Figure 3-34 can be used to develop a relationship to interpolate the H* value of the rank order statistic based on the required estimate given in Table 3-22. The final H* value for the desired rank order statistic is the H* value obtained from the interpolation of the bounding H* values plus the crevice pressure adjustment. Figure 8-1 in References 3-1 and 3-2 shows the crevice pressure distribution adjustment curves for the Model F and Model D5 SGs, respectively.

The order statistic for higher confidence intervals (e.g., 95%) is calculated using a method described in Reference 3-14. This method involves calculating the difference in rank order between the 95/50 probability and confidence estimate and the next highest probabilistic estimate value (e.g., 96%) using standard equations and error functions from Reference 3-14. The final H* value for the desired rank order statistic is the H* value obtained from the interpolation of the bounding H* values plus the crevice pressure adjustment.

The difference in the required order statistic for the whole bundle H* estimates and the whole plant H* estimates (see Table 3-22) is based on the population of the tubes in the plant. The number of tubes in a plant depends on the SG model and the number of SGs in a plant. For simplicity, the entire design population of tubes, including currently plugged tubes, is considered. The difference between a whole bundle value of 9500 (95/50) and a whole plant value is defined by the 9500th H* value for the combined results of 10,000 simulations of each SG in the plant. For example, consider a 4-loop plant: Performing the 10,000 trial Monte Carlo simulation four times to represent four different generators yields four different sets of rank order vectors in terms of H*, TS CTE variation and T CTE variation. All four vectors will be similar, but yield slightly different H* values at the same rank order.

The value of the whole plant H* is determined by first calculating four vectors of H* values corresponding to four steam generators. A fifth vector is then produced whose ith element consists of the maximum H* amongst the ith elements of the four beginning vectors. This vector is then sorted, and the rank order statistic for 95/50 is the 9500th value. This value of H* is then searched for in an ordered input vector to determine approximately what rank order statistic for a single steam generator corresponds to the 9500th rank order H* for an entire plant.

To apply the method discussed herein, it is necessary to identify the whole bundle rank order of the H* value that is the same as the 95 percent H* value for the whole plant. For example, the value of the 95% H* for the four SGs in a Model F plant is equivalent to the [ ]^{a,c,eth} H* value for a single Model F bundle. Other models of SGs have different tube populations than the Model F; therefore, the equivalent rank order for the different model SG will also be different. The difference between the whole bundle H* value and the whole plant H* value comes from using the tube and tubesheet CTE values associated with the H* value for the whole plant 95 percent in the calculations using the C^2 model.

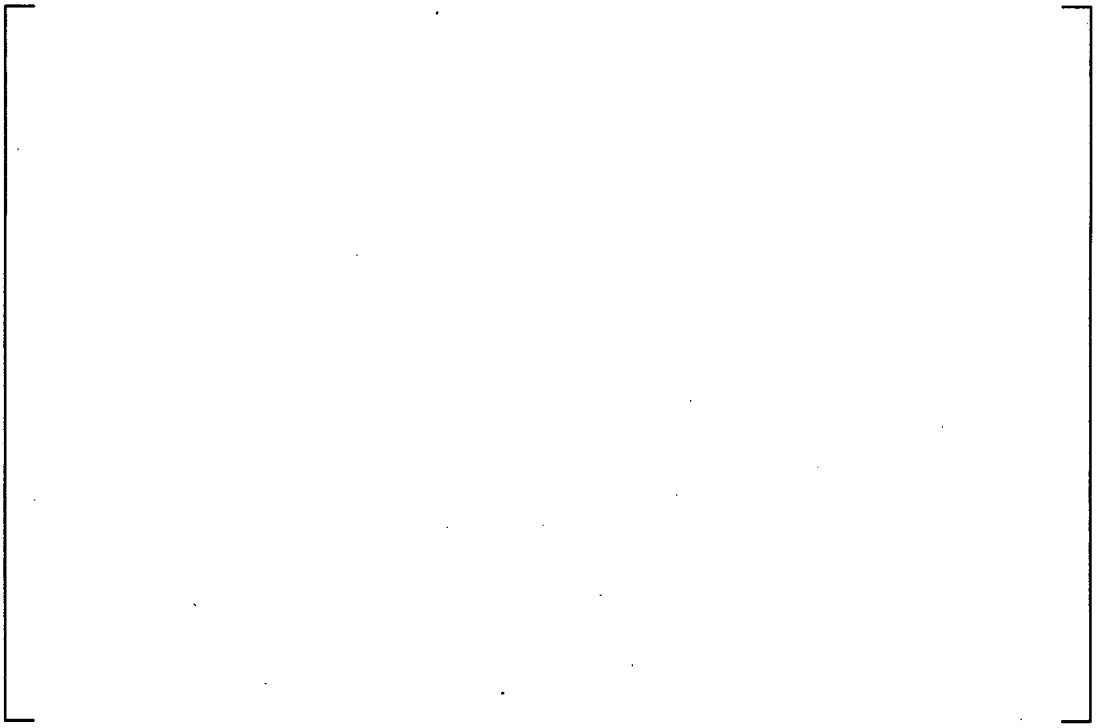

a,c,e

Figure 3-30: Model F Crevice Pressure Adjustment Curve

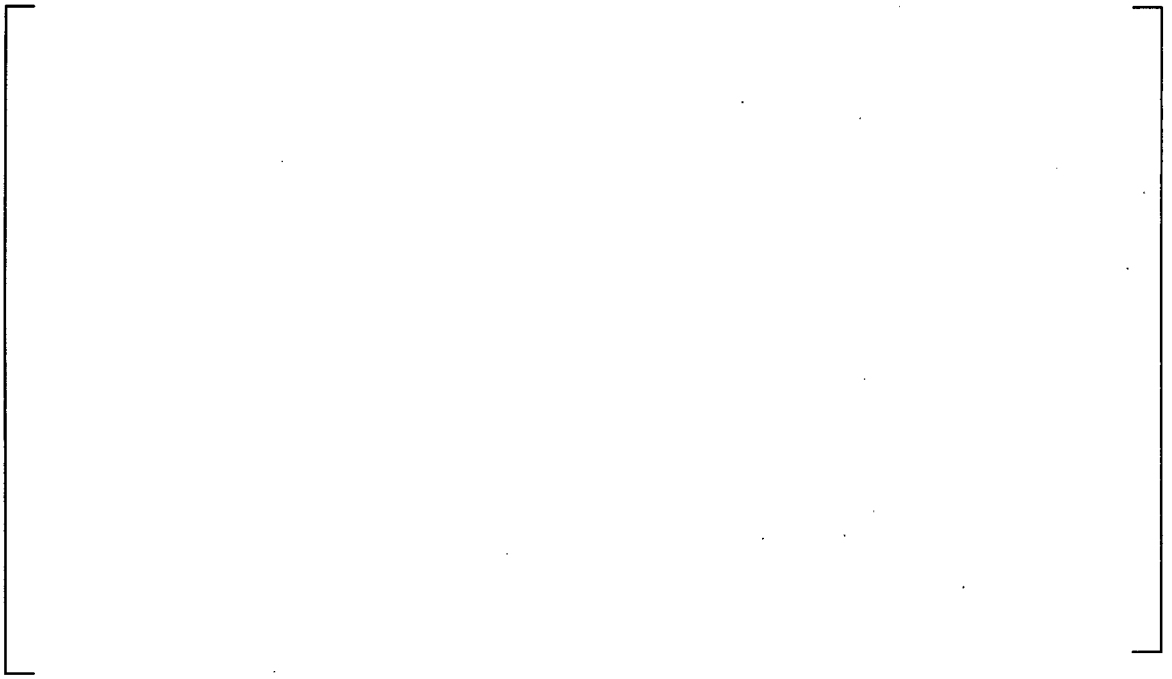

a,c,e

Figure 3-31: Model D5 Crevice Pressure Adjustment Curve

3.4.3 Input

The necessary input for the probabilistic analysis using the C^2 model are:

- The limiting radius for H* for the model SG of interest. The limiting tubesheet radius is the radial position on the tubesheet where the longest H* distance occurs at the limiting operating condition at mean material properties.
- The limiting operating condition for H* (NOP or SLB).
- The significant material properties, CTE for the tubesheet and tube material.

Table 3-24 specifies the limiting radius for H* for the Model F and Model D5 SGs. The limiting radii for the different models of SG were determined using the C^2 model and mean material properties as was done with the thick shell model in the licensing basis analysis. The limiting tubesheet radius was determined to be the same as in the current licensing basis for the Model D5 SGs; however, the limiting radius for the Model F SGs changed to [ ]^{a,c,e} inches based on the C^2 model compared to [ ]^{a,c,e} inches in the current licensing basis (Reference 3-1). Note that in the current licensing basis for the Model F, the H* values at [ ]^{a,c,e} inches radius and at [ ]^{a,c,e} inches radius are very nearly the same. In Table 6-23 of Reference 3-1 the mean H* value at a radius of [ ]^{a,c,e} inches was [ ]^{a,c,e} inches and the mean H* value at a radius of [ ]^{a,c,e} inches was [ ]^{a,c,e} inches, a difference of less than [ ]^{a,c,e} inch. Thus, it is reasonable that application of a different structural model, the C^2 model, could results in this change in critical radius. The sensitivity of H* at both radii is also likely to be similar to the H* values at the [ ]^{a,c,e} inch TS radius. Therefore, the currently developed sensitivities for H* at the [ ]^{a,c,e} inch TS radius can be applied to the H* values calculated at the [ ]^{a,c,e} inch TS radius. Table 3-24 also specifies the limiting operating conditions for the Model F and Model D5 SGs.

The limiting operating condition for H* is the operating condition that produces the most conservative (i.e., longest) predicted H* depth. The operating conditions considered are normal operating condition at low temperature (average conditions), NOP or $NOP_{LOW\ TAVG}$, and main steam line break, SLB, consistent with the current licensing basis.

Typical upper 90th percentile Monte Carlo results are shown in Table 3-25, with the result of the combined value of the tube and tubesheet CTE in the fifth column of the table. The Monte Carlo results cover one thousand rank values (from the 90th percentile to the 100th percentile of 10,000 simulations) based on the Monte Carlo sampling performed in the current licensing basis. The values used in the analysis, and the exact rank order statistics required for the comparison of the H* values generated by the square cell analysis to the H* values in the existing licensing basis are given in Table 3-22 and Table 3-23. The typical range of values for the combined variable for all steam generators is between three and six.

The data in Table 3-23 were selected based on examining the reduced response surface from the existing licensing basis. The reduced response data for the Model F and Model D5 SGs are shown in Figure 3-35 and Figure 3-36 for the NOP condition. For the Model D5 SG, for the limiting SLB conditions, the reduced response data is shown in Figure 3-38 and Figure 3-39. The bounding data in the reduced set from each of the reduced response data plots used to estimate the H* values are listed in Table 3-25. The

CTE variations for the tube and tubesheet materials used in the finite element analyses of the lower SG complex and the square cell analysis are given in Table 3-26 and Table 3-27.

The result of using the material properties in Table 3-26 in the finite element analysis of the lower SG complex is the tubesheet displacement as a function of elevation. This result, along with the variation in the tube properties described in Table 3-27 is used as input to the square cell analysis. The output from the square cell analysis is the contact pressure distribution between the tube and the tubesheet as a function of elevation. This contact pressure distribution is used to calculate the H* values for the response surface comparison. A Poisson offset is also added to the final H* values in order to account for the effect of including an end-cap load on the tube in the C^2 analysis for H* (see Section 3.5 for discussion). An end-cap load physically applied to the tube would act to reduce the outer diameter of the tube by reducing the tube cross section. Application of the Poisson adjustment is conservative because of the counter-acting effect of Poisson expansion due to thermal axial expansion of the tube and bending of the tube portion within the tubesheet are ignored. The Poisson offset is added to the H* result before the crevice pressure adjustment is determined because the Poisson adjustment is constant on the tube regardless of the final tube length as determined by the crevice pressure adjustment.

3.4.4 Model F Results

The H* values (without a crevice pressure adjustment) from the contact pressure distributions developed using the C^2 model at the limiting TS radius are shown in Table 3-28 together with the rank order of the input values as discussed above.

The results shown in Table 3-28 are represented graphically in Figure 3-37. There is a difference in the existing licensing basis results for H* at the given rank order statistics and the square cell model results. The H* estimates based on the square cell model results are about two to three inches greater than those from the licensing basis. The linear fit between the H* results for rank order [ ]^{a,c,e} and [ ]^{a,c,e} is very good, but there is a slight deviation from a perfect fit ($R^2 < 1$) such that a slight decrease in slope occurs from rank order [ ]^{a,c,e} to [ ]^{a,c,e} if two separate linear fits are made of the data.

The linear fit used to interpolate the exact value of H* at the desired rank order statistic for the Model F SG is given by the following equation:

H* Value = [ ]^{a,c,e} (Equation 3-7)

The final values of H*, with the corresponding crevice pressure length adjustment taken from Reference 3-2, are shown in Table 3-29.

3.4.5 Model D5 Results

The contact pressure results from the Model D5 square cell analysis are based on the selected rank order statistics from the Model D5 Monte Carlo (MC) analysis. A Monte Carlo analysis for the Model D5 SLB condition was not included in the existing licensing basis for H* because of the alternate method previously used in structural analysis of the SLB condition in Reference 3-2. Consistent application of a single model, the C^2 model, to the Model D5 SGs showed that the SLB condition is limiting, confirming the results of consistent application of the thick shell model for the Model D5 SGs in the current licensing

basis. Because the SLB condition is the limiting condition, a separate response surface (similar to Figure 8-5 of Reference 3-2) and Monte Carlo simulation were developed to support the probabilistic H* analysis for the Model D5 SGs based on application of the square cell model analysis. The process of developing the response surface was the same as described in the current licensing basis and is documented in Reference 3-13. The resulting H* values at the desired rank order statistics, without any crevice pressure adjustment, from the SLB contact pressure distributions at the limiting TS radius are shown in Table 3-30 for both the licensing basis method and application of the square cell model.

The results shown in Table 3-30 are represented graphically in Figure 3-40. There is approximately a 2.0 inch difference between the updated Monte Carlo SLB results for H* at the given rank order statistics and the square cell model results. The H* estimates for SLB with the square cell model show a slightly positive slope with increasing rank order. The linear fit used to interpolate the value of H* at the desired rank order statistic for the Model D5 SG is given by the following equation:

$$\text{H* Value} = [\quad]^{a,c,e} \qquad \text{(Equation 3-8)}$$

The final values of H*, with the corresponding crevice pressure length adjustment taken from Figure 3-31 are shown in Table 3-31. The final values for the Model D5 H* at different probabilities and confidence estimates using the C^2 model are different from the Model D5 H* values in WCAP-17072-P. This is because the boundary conditions during NOP are different from the boundary conditions applied to the models during SLB. For example, the temperature of the tubesheet during SLB (Primary fluid temperature = [ ]^{a,c,e} °F) is lower than the temperature of the tubesheet during NOP (Primary fluid temperature = [ ]^{a,c,e} °F), which results in smaller tubesheet displacements. The end cap load used to calculate H* during SLB ($1.4\Delta P_{SLB}$ = [ ]^{a,c,e} lbf) is also less than the end cap load used to calculate H* during NOP ($3.0\Delta P_{NOP}$ = [ ]^{a,c,e} lbf). The net effect is that the SLB results use a different contact pressure distribution that is less sensitive to variations in CTE even though the mean H* value for SLB condition is larger than the mean NOP H* value.

a,c,e

Figure 3-32 Typical Result for Plotting the Combined Tube and Tubesheet, CTE Values Against H* from the Licensing Basis Analysis

a,c,e

Figure 3-33 Typical Result for Plotting the Combined Tube and Tubesheet, CTE Values Against Monte Carlo Rank Order from the Licensing Basis Analysis

a,c,e

Figure 3-34 Typical Comparative H* Curves from Selected Response Surface

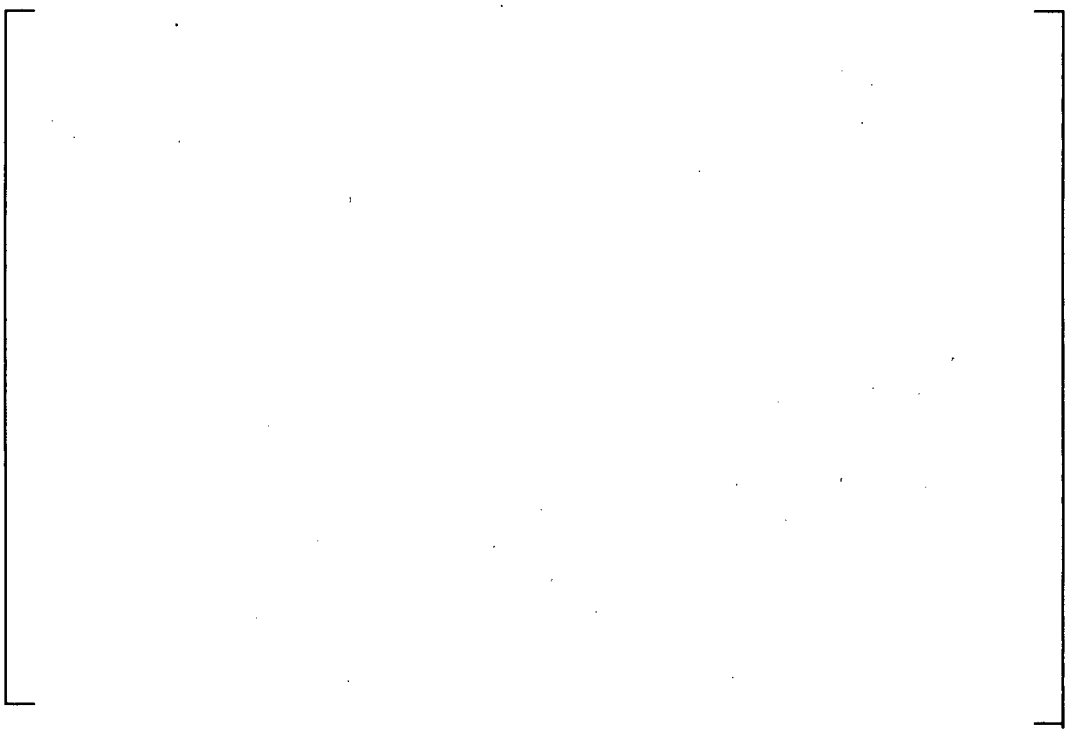

a,c,e

Figure 3-35 Model F NOP Combined CTET and CTETS vs. Monte Carlo Rank Order

a,c,e

Figure 3-36 Reduced Model F NOP Response Data

a,c,e

Figure 3-37 Model F H* Summary Showing Linear Fit Results

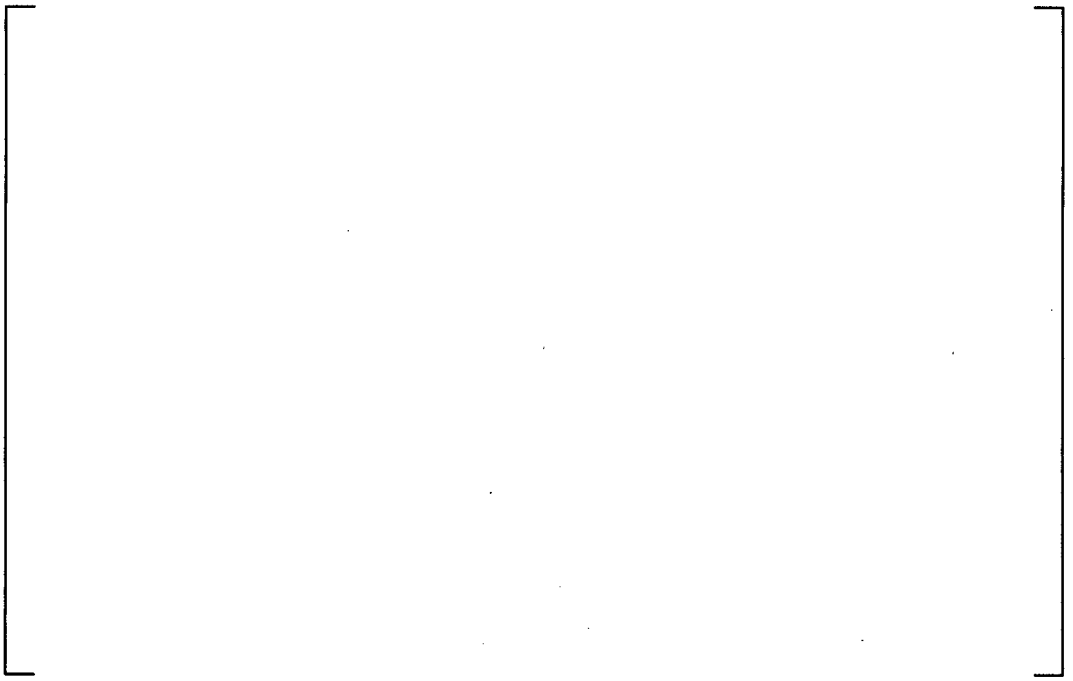

a,c,e

Figure 3-38 Model D5 SLB Combined T CTE and TS CTE as a Function of H*

a,c,e

Figure 3-39 Reduced Model D5 SLB Response Data

a,c,e

Figure 3-40 Model D5 H* Summary Showing Linear Fit Results

Table 3-22 Required Probabilistic Estimate for H*

Model SG	Whole Bundle Estimate		Whole Plant Estimate	
	95/50	95/95	95/50	95/95
F				
D5				
44F				
51F				

a,c,e

Notes:

(1) Whole plant does not apply because SLB is limiting condition for H*

(2) Values are the whole bundle rank orders based on whole plant rank order equivalent H* to recover the corresponding values of tube and tubesheet CTE.

Table 3-23 Monte Carlo Data Used in Comparative Probabilistic Analysis

Model SG	Limiting Operating Condition	Rank Order Statistic (1)	Tubesheet CTE Variation (standard deviations)	Tube CTE Variation (standard deviations)	Alpha
F	NOP				
D5	SLB				
44F 3-Loop	NOP				
51F	NOP				

a,c,e

Notes: (1) Based on 10,000 simulations

Table 3-24 Limiting Operating Condition and TS Radius for H* Square Cell Analysis

SG Model	Limiting TS Radius (in.)	Limiting Operating Condition
F	[ ]^{a,c,e}	NOP
D5	[ ]^{a,c,e}	SLB$^{(1)}$
Notes; 1. Changed from current licensing basis 2. Same as current licensing basis		

Table 3-25 Typical Monte Carlo Result Output

Rank #	HSTAR	NSIG_T	NSIG_TS	Alpha

a,c,e

Table 3-26 Positive Variations about the Mean TS CTE Used for FEA

(Units of 10-6 in/in/°F)

Temp. °F	Mean	Multiplier on Standard Deviation					
70	6.50						
200	6.67						
300	6.87						
400	7.07						
500	7.25						
600	7.42						
700	7.59						

a,c,e

Table 3-27 Negative Variations about the Mean Tube CTE used for FEA

(Units of 10-6 in/in/°F)

Temp. °F	Mean	Multiplier on Standard Deviation										
212	7.22											
300	7.40											
420	7.60											
500	7.70											
600	7.82											
628	7.85											

a,c,e

Table 3-28 Bounding Model F H* Results for Comparison Study

(without Pcrev Adjustment)

MC Rank in 10K Simulations	H* Result from Current Licensing Basis in.	H* Result from Square Cell Analysis in.

a,c,e

Table 3-29 Summary of Model F Probabilistic Estimates

Description -	MC Rank in 10K Simulations	H*- C^2 (in.)	P_{crev} (in.)	Poisson Offset (in.)	Final (in.)
Whole Plant, 95/50	[				]a,c,e 15.15
Whole Plant, 95/95					15.20
Whole Bundle, 95/50					14.57
Whole Bundle, 95/95					14.60

Table 3-30 Bounding Model D5 H* Results for Comparison Study

MC Rank in 10K Simulations	H* Result from Licensing Basis MC Study (in.)	H* Result from Square Cell Analysis (in.)
[		] a,c,e

Table 3-31 Summary of Model D5 Probabilistic Estimates

Name -	MC Rank #	H*- C^2 (in.)	P_{crev} (in.)	Poisson Offset (in.)	Final (in.)
Whole Bundle, 95/50	[			] a,c,e	13.35
Whole Bundle, 95/95					13.36

3.5 POISSON CONTRACTION EFFECT ON H*

An evaluation was performed to determine the effect of end cap loading on H* due to Poisson contraction of the tube. The pressure differential across the tube wall creates an effective end cap load, generating a positive axial stress state in the tube. This will cause a radial contraction of the tube via Poisson's ratio, which will necessarily reduce the contact pressure between the tube and tubesheet, hence increasing H*. The purpose of this section of the report is to address the impact of Poisson contraction on the values calculated for H* using the C^2 model.

3.5.1 Methods Discussion

The method used to evaluate the effect of Poisson's ratio on H* is a simplified approach using approximations to determine the reduction in contact pressure. A classical thick-shell formula is used to calculate the change in radius due to Poisson's ratio effects from an applied end cap load. This change in radius is directly converted to a contact pressure utilizing the thick shell equations in Reference 3-2. This contact pressure is then subtracted from the contact pressure curve calculated in Reference 3-8 and summarized above. The difference is reported and discussed. All calculations for Poisson's contraction are based on an end cap load without a factor of safety, as it is unrealistic to apply a factor of safety to a physical effect such as Poisson's contraction. The end cap load used to generate H*, however, continues to include the appropriate factor (3.0 for 100 percent power, 1.4 for SLB).

3.5.2 Discussion of Significant Assumptions

The limiting plant for each model SG, as defined in References 3-1 and 3-2 is assumed to have the limiting Poisson effect. This is reasonable because, in part, the limiting plant is determined by that with the highest end cap load.

100 percent Power and SLB were determined to be the limiting conditions in References 3-1 and 3-2 for H*. Consistent with those analyses, these two conditions are examined. The long-term steady-state portion of the SLB transient is analyzed statically, which is reasonable because this portion of the transient continues for hours.

3.5.3 Input

The input for this analysis consists of steam generator dimensions for the plants to be analyzed, material properties from the ASME code, and pressure and temperature conditions from the PCWG parameters and transients.

The end cap loads for the different model SGs, Table 3-32, are taken from References 3-1 and 3-2. The modulus of elasticity is in the same as in the FEA, in Table 3-3. Poisson's ratio for Alloy 600 is [ ]^{a,c,e} as taken from the ASME code, Reference 3-12.

Material properties were taken at temperatures consistent with those used in the FEA discussed in Section 3.1. Material properties are taken at [ ]^{a,c,e}°F for 100 percent power for all plants. For the Model D5 SLB analysis, properties were taken at [ ]^{a,c,e}°F.

3.5.4 Calculation of Radial Dilation

From Reference 3-17 (Page 396), the radial dilation of a pressurized thick-wall cylinder is given by

$$\Delta R = \frac{r}{E_t\left(r_o^2 - r_i^2\right)}\left[\left(1-2\nu\right)\left(p_i r_i^2 - p_o r_o^2\right) + \left(1+\nu\right)\frac{r_i^2 r_o^2\left(p_i - p_o\right)}{r^2} - \frac{\nu P}{\pi}\right] \qquad \text{(Equation 3-10)}$$

Where,

P = Endcap load (pounds)

ν = Poisson's ratio

r = Radial coordinate (inches)

r_o = Outer radius of tube (inches)

r_i = Inner radius of tube (inches)

p_i = Pressure on inside of tube (psi)

p_o = Pressure on outside of tube (psi)

E_t = Elastic Modulus of tube (psi)

π = pi (3.14159265358979323)

ΔR = change in radial coordinate due to loadings (inches)

P is the end cap load, in pounds. Since the figure of interest is the radial contract at the outside radius due to the applied end cap load, the difference is:

$$\Delta R_{endcap} = -\frac{r_o \nu P}{E\pi\left(r_o^2 - r_i^2\right)} \qquad \text{(Equation 3-11)}$$

This equation is used to calculate radial dilations in due to the Poisson contraction alone (Table 3-32). As can be seen, there is a small radial contraction (approximately [ ]^{a,c,e} micro-inches) due to Poisson effects.

3.5.5 Calculation of Contact Pressure Reduction from Poisson Effect

The contact pressure change due to Poisson effects can be estimated by using the Thick Shell Equations from References 3-1 and 3-2. The thick shell formula is (page 6-87 of Reference 3-1):

[ ] a,c,e

(Equation 3-12)

Where,

P_i = Internal primary side pressure, psi

P_{crev} = Crevice pressure, psi

r_i = Inside radius of tube, in

r_o = Outside radius of tube, in

α_t = Coefficient of thermal expansion of tube, in/in/°F

E_t = Modulus of Elasticity of tube, psi

E_{ts} = Modulus of Elasticity of tubesheet, psi

T_t = Temperature of tube, °F, and,

ν = Poisson's Ratio of the material.

$P_{contact}$= Contact Pressure

D = Outside radius of cylinder which provides the same radial stiffness as the tubesheet

As can be seen, the thick shell equation for contact pressure is simply a sum of radial displacements divided by an effective elastic constant. This makes intuitive sense because the physical interpretation of the thick shell equations is as follows:

1. Apply internal pressure, crevice pressure, and thermal loads to a free tube which has a nominal outside diameter equivalent to the collar bore ID. Calculate the resultant radial dilation.
2. Calculate the bore displacement of a free collar from crevice pressure and the applied dilation from the 3-D FEA model.
3. If the answers to one and two above possess a geometric interference (the resultant tube radius is larger than the bore), then there exists positive contact pressure. The positive contact pressure can be calculated as that pressure which, when applied to both the tube OD and the collar ID, eliminates the geometric interference, producing line-on-line contact.

In step 3, it is clear that the relationship between contact pressure and radial geometric interference should be linear, as the thick shell equations are linear elastic. Therefore, it is appropriate to calculate contact pressure reduction by simply dividing the differential radial displacement due to Poisson's ratio effects by the elastic constant in the denominator above:

[ ]^{a,c,e}

(Equation 3-13)

Results of the calculation of the elastic constants are provided in Table 3-33 for Model F and Model D5 SG operating conditions. Substituting the differential radial dilation from Table 3-32 into the above equation yields the contact pressure reductions shown in Table 3-34. As can be seen, there are modest reductions of approximately [ ]^{a,c,e} psi at 100% power and approximately twice that (~[ ]^{a,c,e} psi) at SLB conditions. This makes intuitive sense because the Poisson' contraction is proportional to the stress, which is proportional to the pressure differential, and the SLB delta-p is approximately twice that of 100% power.

3.5.6 Calculation of Increase in H* Values

In order to calculate the change in H* values due to the decreased contact pressure, the contact pressure curves from Section 3.3 must be reduced by the above contact pressures and integrated again to find the change in H*. In each case, only the critical radius will be evaluated for each model. For the D5 Steam Generators, both 100% Power and SLB are analyzed to show how the contact pressure affects SLB and also because SLB has been determined to be the limiting condition for the D5 Steam Generators. The reference square cell analysis explains the methodology for calculating H*. The formula for pull out load is:

$$F = \int \mu \pi d_o P_{contact} dy \qquad \text{(Equation 3-14)}$$

Where μ is the coefficient of friction, chosen to be [ ]^{a,c,e} in the licensing basis analysis. Calculations for the increased H* for each model are in Table 3-35 and Table 3-36, and a sample chart is in Figure 3-41. In each case, the contact pressure curve is shifted down by the appropriate amount and H* recalculated. Baseline numbers from Reference 3-9 are included for comparison. As can be seen, the increase in H* due to Poisson effects amounts to approximately [ ]^{a,c,e} inches (before attenuation). This value assumes Poisson contraction occurs along the entire length. A more realistic calculation will account for the Poisson effect attenuating after an accumulated pull out resistance equal to the end cap load is attained. This correction is obtained by interpolation using the same methodology as for H*, but with an end cap load that does not have a factor of safety. The interpolated attenuation distances are in Table 3-37.

The next step in the process is to calculate new H* values with contact pressures that are reduced only inside the attenuation distance. This involves interpolating the contact pressure and shifting only a portion of it. Calculations are tabulated in Tables 3-38 through 3-40. A summary of the Final H* values after adjusting for Poisson contraction and attenuation are in Table 3-40. As can be seen, the greatest difference is approximately [ ]^{a,c,e} inches.

However, this is for mean H* values. The final figure of interest is the effect that Poisson contraction has on the probabilistic, or extreme H* values. Calculations for the probabilistic values are in Table 3-41

through Table 3-45. A summary of the effect of Poisson's contraction on H* is in Table 3-46. As can be seen, the largest effect is [ ]^{a,c,e} inch for the Model F SG ([ ]^{a,c,e} inch for the Model D5).

Table 3-32 Calculation of Radial Dilation Due to Poisson Effects Model F and D5 SGs

Parameter	Model F	Model D5	
	100% Power	100% Power	SLB
Tube R_i (in)	[		] a,c,e
Tube R_o (in)			
E_{tube} (Msi)			
Endcap Load (lbs) (1)			
Delta-R (micro-inch)			]
(1) End cap load based on NOP ΔP			

Table 3-33 Calculation of Elastic Constants All Model SGs

Parameter	Model F		Model D5	
	100% Power	SLB	100% Power	SLB
Tube r_i (in)	[			] a,c,e
Tube r_o (in)				
Collar R_o (in)				
Tube E (Msi)				
Tubesheet E (Msi)				
ν				
Elastic Constant (in^3/lb)				]

Table 3-34 Calculation of Reduction in Contact Pressure from Poisson Effects

Parameter	Model F	Model D5	
	100% Power	100% Power	SLB
Δr due to ν (μin)			
Elastic Constant (in^3/lb)			
P_{con} Reduction (psi)			

[ ]a,c,e

Table 3-35 Baseline and Adjusted H* Calculation for Model F (Millstone Unit 3)

Model F, 100% Power, [ ]a,c,e in Radius				
Endcap load = [ ]a,c,e pounds				
Elevation	Baseline		Shifted due to Poisson	
	P_{con} (psi)	Accumulated Pull Out Load (pounds)	P_{con} (psi)	Accumulated Pull Out Load (pounds)
0(1)				
2				
4				
6				
10.515				
16.901				
19.03				
20.03				
21.03(2)				
H* (inches)				

[ ]a,c,e

Notes:
(1) Bottom of the Tubesheet
(2) Top of the Tubesheet

Table 3-36 Baseline and Adjusted H* Calculation for Model D5 (Byron Unit 2)

Model D5, SLB, [ ]^{a,c,e} in Radius					
Endcap load = [ ]^{a,c,e} pounds					
Elevation	Baseline		Shifted due to Poisson		
	P_{con} (psi)	Accumulated Pull Out Load (pounds)	P_{con} (psi)	Accumulated Pull Out Load (pounds)	a,c,e
0[1]					
2					
4					
6					
10.515					
16.901					
19.03					
20.03					
21.03[2]					
H* (inches)					

Notes:
(1) Bottom of the Tubesheet
(2) Top of the Tubesheet

Table 3-37 Distance for Poisson Effect to Attenuate

Model SG	F	D5 SLB
Distance for Poisson Effect to Attenuate (inches)	[	]^{a,c,e}

Table 3-38 H* Calculation for Model F Including Poisson Attenuation (Millstone Unit 3)

Model F, 100% Power, [ ]^{a,c,e} in Radius		
Endcap load = [ ]^{a,c,e} pounds		
Elevation	**P_{con} (psi)**	**Accumulated Pull Out Load (pounds)**
$0^{(1)}$	[	] ^{a,c,e}
2		
4		
6		
10.515		
15.277		
16.901		
19.03		
20.03		
$21.03^{(2)}$		
H* (inches)		

Notes:
(1) Bottom of the Tubesheet
(2) Top of the Tubesheet

Table 3-39 H* Calculation for Model D5 including Poisson Attenuation (Byron Unit 2)

Model D5, SLB, [ ]^{a,c,e} in Radius		
Endcap load = [ ] ^{a,c,e} pounds		
Elevation	**P_{con} (psi)**	**Accumulated Pull Out Load (pounds)**
$0^{(1)}$	[	] ^{a,c,e}
2		
4		
6		
10.515		
13.61		
16.901		
19.03		
20.03		
$21.03^{(2)}$		
H* (inches)		

Notes:
(1) Bottom of the Tubesheet
(2) Top of the Tubesheet

Table 3-40 Comparison of Mean H* Values

Parameter	Model F	Model D5 SLB
H* Unmodified	[	] a,c,e
H* + Poisson		
H* + Poisson + Attenuation		
Final Difference		

Table 3-41 Baseline and Adjusted H* Calculation for Model F (Millstone Unit 3)

(MC rank [ ]^{a,c,e})

Model F, 100% Power, [ ]^{a,c,e} in Radius				
Endcap load = [ ]^{a,c,e} pounds				
Elevation	**Baseline**		**Shifted due to Poisson**	
	P_{con} (psi)	**Accumulated Pull Out Load (pounds)**	**P_{con} (psi)**	**Accumulated Pull Out Load (pounds)**
0(1)	[			] a,c,e
2				
4				
6				
10.515				
16.901				
19.03				
20.03				
21.03(2)				
H* (inches)				

Notes:
(1) Bottom of the Tubesheet
(2) Top of the Tubesheet

Table 3-42 Baseline and Adjusted H* Calculation for Model D5 (Byron Unit 2)

(MC Rank [ ]^{a,c,e})

Model D5, SLB, [ ]^{a,c,e} in Radius				
Endcap load = [ ]^{a,c,e} pounds				
Elevation	**Baseline**		**Shifted due to Poisson**	
	P_{con} (psi)	**Accumulated Pull Out Load (pounds)**	**P_{con} (psi)**	**Accumulated Pull Out Load (pounds)** ^{a,c,e}
0[1]				
2				
4				
6				
10.515				
16.901				
19.03				
20.03				
21.03[2]				
H* (inches)				

Notes:
(1) Bottom of the Tubesheet
(2) Top of the Tubesheet

Table 3-43 Distance for Poisson Effect to Attenuate Probabilistic H* Values

Model SG	F	D5 SLB
Distance for Poisson Effect to Attenuate (inches)	[	]^{a,c,e}

Table 3-44 H* Calculation for Model F Including Poisson Attenuation (Millstone Unit 3)

(MC rank [ ]^{a,c,e})

Model F, 100% Power, [ ]^{a,c,e}" Radius				
Endcap load = [ ]^{a,c,e} pounds				
Elevation	**P_{con} (psi)**		**Accumulated Pull Out Load (pounds)**	
0[1]				a,c,e
2				
4				
6				
10.067				
10.515				
16.901				
19.03				
20.03				
21.03[2]				
H* (inches)				

Notes:
(1) Bottom of the Tubesheet
(2) Top of the Tubesheet

Table 3-45 H* Calculation for Model D5 including Poisson Attenuation (Byron/Braidwood Unit 2)

(MC rank [ ]^{a,c,e})

Model D5, SLB, [ ]^{a,c,e} in Radius		
Endcap load = [ ]^{a,c,e} pounds		
Elevation	**P_{con} (psi)**	**Accumulated Pull Out Load (pounds)** a,c,e
0(1)		
2		
4		
6		
10.35		
10.515		
16.901		
19.03		
20.03		
21.03(2)		
H* (inches)		

Notes:
(1) Bottom of the Tubesheet
(2) Top of the Tubesheet

Table 3-46 Comparison of Probabilistic H* Values (inches)

Parameter	Model F	Model D5 SLB
H* Unmodified		
H* + Poisson		
H* + Poisson + Attenuation		
Final Difference		

a,c,e

a,c,e

Figure 3-41 Effect of Poisson Contraction on Contact Pressure

3.6 REFERENCES

3-1. WCAP-17071-P, Revision 2, "H*: Alternate Repair Criteria for the Tubesheet Expansion Region in Steam Generators with Hydraulically Expanded Tubes (Model F)," September 2010.

3-2. WCAP-17072-P, "H*: Alternate Repair Criteria for the Tubesheet Expansion Region in Steam Generators with Hydraulically Expanded Tubes (Model D5)," May 2009.

3-3. WTD-SM-75-072, "Temperature Distributions for Calculation of Secondary Skin Stress in D2-D3 Tubesheet Analysis," August 1975.

3-4. Report 1014982, "Divider Plate Cracking in Steam Generators: Results of Phase I: Analysis of Primary Water Stress Corrosion Cracking and Mechanical Fatigue in the Alloy 600 Stub Runner to Divider Plate Weld Material," EPRI, Palo Alto, CA; 2007.

3-5. Jaluria, Yogesh, "Computer Methods for Engineering," Taylor and Francis, 1996.

3-6. CN-SGMP-10-15, Revision 1, "3-D Finite Element Analysis of Limiting Plants for H* with Thermal Profile," November 2010.

3-7. WNET-150, Volume 3, "Model E2, Steam Generator Stress Report, Primary Chamber Components Interactions Analysis," December 1978.

3-8. CN-SGMP-10-3, Revision 1, "Square Cell Finite Element Analyses for Models D5, F, 44F and 51F Plants for H*," November 2010.

3-9. LTR-SGMP-09-104, Revision 1 "White Paper: H* Values at More Restrictive Probabilistic Criteria," August 13, 2009.

3-10. A.C. Atkinson, *The Design of Experiments to Estimate the Slope of a Response Surface*, Biometrica 1970, Volume 57, Issue 2, pg. 319.

3-11. CN-SGMP-10-18, "H* Analysis Using Thick-Shell Equations for Byron/Braidwood Unit 2 and Point Beach Unit 1 for Steam Line Break Conditions," October 11, 2010

3-12. ASME B&PV Code, 2007 Edition, No Addenda, Section II, Part D, Subpart 2: Physical Properties Tables, Table PRD.

3-13. LTR-SGMP-09-100 P-Attachment, Revision 1 "Response to NRC Request for Additional Information on H*; Model F and Model D5 Steam Generators," September 7, 2010.

3-14. *Statistics, Probability and Reliability for Civil and Environmental Engineers*, Kottegoda, N.T., Rosso, R., McGraw-Hill, © 1997.

3-15. Westinghouse Drawing 1105J05, Revision 3, "Tube Plate Drilling."

3-16. LTR-SGMP-10-135 Assessment of Feedline Break Conditions on Contact Pressures for Model F for H*, 10/26/10.

3-17. *Advanced Mechanics of Materials*, Boresi, Arthur P and Schmidt, Richard J, Sixth Edition, John Wiley and Sons Publishing

4 C^2 MODEL LEAKAGE INTEGRITY DISCUSSION

The model for leakage applied in References 4-1, 4-2 and 4-3 is the Darcy formulation for leakage through a porous medium. The Darcy equation is:

$$Q = \frac{\Delta p}{12 \mu K l} \qquad \text{(Equation 4-1)}$$

Where:

Δp is the driving potential (primary to secondary pressure difference)

μ is the fluid dynamic viscosity

K is the loss coefficient for flow through the porous medium

l is the length of the porous medium

The Darcy formulation (Eq. 4-1) is used in References 4-1, 4-2 and 4-3 to develop the ratio of leak rates between postulated accident induced conditions and normal operating conditions (NOP). The resulting Darcy flow equation ratio can be separated into four "subfactors" as follows:

$$\frac{Q_{DBA}}{Q_{NOP}} = \frac{\Delta p_{DBA}}{\Delta p_{NOP}} \frac{\mu_{NOP}}{\mu_{DBA}} \frac{K_{NOP}}{K_{DBA}} \frac{l_{NOP}}{l_{DBA}} \qquad \text{(Equation 4-2)}$$

The purpose of this section of the report is to address the impact of the new square cell model results on the existing licensing basis leak rate factors provided in Reference 4-3 for the Model F and Model D5 steam generators. Among the four leakage subfactors identified in Equation 4-2 above, it has been determined that the latest square cell model results affect two of the four subfactors for the Model D5 steam generator only. The subfactors affected are the loss coefficient subfactor (K_{NOP}/K_{DBA}) and the effective crevice length subfactor (l_{NOP}/l_{DBA}). The driving heads (Δp) at both of these conditions are known, as are the temperatures and pressures to define the fluid viscosity (μ). As discussed in References 4-1 and 4-2, the design specification curves for the locked rotor and control rod ejection events apply for the leakage factors for these transients. These transients are of very short duration, for which the H* leakage calculations employ a time integrated leakage approach. The same leakage factors for a postulated locked rotor and control rod ejection event for the Model D5 and F SGs in the H* fleet included in Reference 4-3 continue to apply.

4.1 LOSS COEFFICIENT SUBFACTOR DISCUSSION

4.1.1 Model D5 AND F SG SLB Condition

As discussed in Section 9.1.1 of References 4-1 and 4-2, the current licensing basis leakage factors assume a loss coefficient subfactor of 1.0. The available data for hydraulically expanded tubes in tubesheet simulants (References 4-4 and 4-5), both at room temperature and at elevated temperature, are utilized in References 4-

1 through 4-3 to show that no correlation between loss coefficient and contact pressure exists for conditions that simulate the Model D5 SG conditions. However, because the data exhibit considerable scatter, confidence in this data analysis is low. Engineering judgment could suggest that loss coefficient might be related to the absolute contact pressure between the tubes and the tubesheet. Hence, a requirement was applied to the H* leakage analysis by the regulatory authorities that it is necessary to show that the contact pressure at accident induced conditions exceeds the contact pressure at normal operating conditions ($Pc_{FLB/SLB}$:Pc_{NOP}>1) in order to assume that the loss coefficient subfactor is equal to 1.0. Only the Model D5 is of concern because it cannot be shown that contact pressure at SLB conditions exceeds that at NOP conditions for the Model D5. For the Model F, the SLB contact pressure exceeds the NOP contact pressure in all cases.

The calculated contact pressure results for all models of SG are, to a large degree, dependent on the temperatures at a particular operating condition. The licensing basis for the Model D5 SG includes a SLB condition that differs from the SLB conditions in the licensing basis for the other SG models. The Model D5 SG SLB transient includes a significantly lower temperature; as a result, it cannot be shown that the contact pressures at accident conditions exceed those at normal operating conditions, and the criterion for contact pressure ($Pc_{FLB/SLB}$:Pc_{NOP}>1) is not met. Consequently, it is necessary to utilize a different approach for leakage analysis that does not depend on loss coefficient being independent of contact pressure to show that the accident induced leakage value assumed in the FSAR is not exceeded.

Concerning the Model D5 steam generators, it has been determined using both thick shell equations and the C^2 model that the contact pressures during steam line break conditions at various elevations between 0 and 21.03 inches at certain radii in the tube bundle does not always exceed the contact pressures during NOP conditions and, therefore, the criterion $Pc_{FLB/SLB}$:Pc_{NOP}>1 is not met. Therefore, it was necessary to determine if the leakage factor for a postulated SLB event remains bounded by the leakage factor for a postulated FLB.

As discussed in detail in Reference 4-6, this involved the development of two alternate approaches for calculating a SLB leakage factor when SLB contact pressures are reduced relative to normal operating condition contact pressures.

The alternate approaches considered were:

1. Parametric assumptions of loss coefficient dependency on contact pressure.

2. Application of parallel plate theory.

Both approaches rely on the existing Model D5 leak rate data to varying degrees. The approach of assuming various proportionality formulations between the loss coefficient and contact pressure and benchmarking them against the existing data is the most direct application. The latter approach utilizes accepted theory to calculate a flow area based on test results and relates that flow area (and consequential leak rate) to the contact pressure conditions for the test specimens to develop leak rates for both SLB and NOP conditions.

Both approaches calculated a SLB leakage factor of less than [ ]^{a,c,e} which remains bounded by the current licensing basis leakage factors for the entire H* fleet with considerable margin. The current licensing basis leakage factors range from 3.11 to 3.27 for a postulated FLB heatup event.

Concerning the Model F steam generators in the H* fleet, the results of the square cell analysis show that the contact pressure during steam line break conditions at various elevations between 0 and 21.03 inches at all radii in the tube bundle always exceeds the contact pressure during normal operating conditions as shown on Figures 3-24 through 3-29 of this report, thereby meeting the criterion ($Pc_{FLB/SLB}$:Pc_{NOP}>1). Therefore, it is concluded that there is no adverse impact on existing values for the leakage factors defined for the Model F SGs (i.e., the leakage factors calculated for a postulated FLB event still bound the leakage factors calculated for a postulated SLB event). The leakage factors remain the same as in the current licensing basis for the Model F SGs.

4.1.2 Model D5 and F Steam Generator Feedline Break Discussion

For the Model D5 SGs, the contact pressures during a postulated FLB event have been calculated at 9 elevations at 6 different radii using the square cell model. It has been determined that FLB contact pressure always exceeds NOP condition contact pressure at all the tube bundle radii and elevations in the tubesheet as shown in Figures 4-1 through 4-6. Therefore, it remains conservative to apply a ratio of K_{NOP}/K_{DBA} of 1.0 and the current licensing basis leakage factors identified in Reference 4-3 continue to apply.

For the Model F SG, the primary differences in boundary conditions between SLB and FLB are an increase in primary pressure from [ ]^{a,c,c} psia to [ ]^{a,c,c} psia, a hot leg temperature increase from [ ]^{a,c,e} °F to [ ]^{a,c,e}°F, and a cold leg temperature increase from [ ]^{a,c,e}°F to [ ]^{a,c,e} °F. The pressure increase will result in a small increase in tubesheet bending, which will have a minor effect on the through-thickness contact pressure profile. The temperature increase will reduce the elastic moduli of the materials by a small amount, which will also increase the bending slightly, again having a minor impact on through-thickness contact pressure profiles. The temperature increase will also increase the differential thermal growth between the tube and the tubesheet. This is expected to result in overall higher contact pressures for feedline break relative to steamline break (Reference 4-8).

Therefore, for the Model F SG, referring to Figures 3-24 to 3-29 of this report, it is observed that SLB contact pressure exceeds the contact pressure during NOP conditions for all radii of the tube bundle the entire thickness of the tubesheet during a postulated SLB (relative to NOP conditions), therefore, as the contact pressures during a postulated FLB would be expected to increase, it is conservative to apply a ratio of K_{NOP}/K_{DBA} of 1.0.

a,c,e

Figure 4-1 Feedline Break Contact Pressure at 4.437 in. Radius

a,c,e

Figure 4-2 Feedline Break Contact Pressure at 10.431 in. Radius

0-TS Elevation is the Top of the Tubesheet

a,c,e

Figure 4-3 Feedline Break Contact Pressure at 18.139 in. Radius

a,c,e

Figure 4-4 Feedline Break Contact Pressure at 26.703 in. Radius

0-TS Elevation is the Top of the Tubesheet

a,c,e

Figure 4-5 Feedline Break Contact Pressure at 42.974 in. Radius

a,c,e

Figure 4-6 Feedline Break Contact Pressure at 49.825 in. Radius

0-TS Elevation is the Top of the Tubesheet

4.2 EFFECTIVE CREVICE LENGTH SUBFACTOR DISCUSSION

4.2.1 Model D5 and F Steam Line Break Discussion

As discussed in References 4-1 and 4-2, recall that "effective crevice length" is defined as the length of positive contact between the tube and the tubesheet (above H*). Based on a review of Figures 3-18 to 3-23 of Section 3.6.11, for the Model D5 steam generators, the latest square cell model analysis results do not show that positive contact pressure exists throughout the thickness of the tubesheet above the H* distance during both NOP and SLB conditions. Therefore, the effective length ratio subfactor for (l_{NOP}/l_{DBA}) cannot be assumed to be 1.0 during a postulated steam line break event for the Model D5 SGs.

To determine the applicable effective length subfactor based on the C^2 model analysis, Figures 3-18 to 3-23 were linearly extrapolated along the slope of the first tubesheet segment from the TTS with a non-zero contact pressure to determine the x-intercept for both the NOP and SLB conditions. The distance of positive contact pressure above the H* distance down from the top of the tubesheet was then determined and a new effective length ratio was calculated. Referring to Table 4-1, four of the 6 radii have effective contact pressure ratios greater than 1.0 using the square cell model results.

Despite the length factor increase, no increase in the current licensing basis leakage rate factors reported in Reference 4-3 is necessary because the increase in effective crevice length ratio is counterbalanced by the reduction in viscosity subfactor ratio which occurs as a result of the reduction in primary fluid temperature from hot standby conditions from [ ]^{a,c,e} °F to [ ]^{a,c,e} °F during a postulated SLB event. The viscosity subfactor ratio decreases to [ ]^{a,c,e} (i.e., [ ]^{a,c,e} lbm/ft-sec / [ ]^{a,c,e} lbm/ft-sec (Reference 4-7) from an assumed value of 1.0; 0.49 times the bounding effective crevice length ratio of 2.02 in Table 4-1 is less than 1.

For the Model F SG, referring to Figures 3-24 to 3-29 of this report, it can be observed that there is positive contact pressure for all radii of the tube bundle the entire thickness of the tubesheet during a postulated SLB (relative to NOP conditions), therefore, the effective crevice length ratio (l_{NOP}/l_{DBA}) is always less than 1.0 above H*.

Moreover, the leak rate factors defined for the Model D5 and F SGs in Reference 4-1 and 4-2 are based on a postulated FLB event, not a postulated SLB.

4.2.2 Model D5 and F Feedline Break Discussion

For the Model D5 SG, as discussed in Section 4.1 of this report, it is shown that a positive contact pressure exists throughout the thickness of the tubesheet at all tube bundle radii. Therefore, based on a review of Figures 4-1 through 4-6, the effective crevice length ratio (l_{NOP}/l_{FLB}) remains less than or equal to 1.0 above H* and there is no impact on the current leakage factors identified in Reference 4-3.

For the Model F SG, the primary differences in boundary conditions between SLB and FLB are an increase in primary pressure from [ ]^{a,c,e} psia to [ ]^{a,c,e} psia, a hot leg temperature increase from [ ]^{a,c,e} °F to [ ]^{a,c,e} °F, and a cold leg temperature increase from [ ]^{a,c,e} °F to [ ]^{a,c,e} °F. The pressure increase will result in a small increase in tubesheet bending, which will have a minor effect on the through-thickness contact pressure profile. The temperature increase will reduce the elastic moduli of the materials by a small

amount, which will also increase the bending slightly, again having a minor impact on through-thickness contact pressure profiles. The temperature increase will also increase the differential thermal growth between the tube and the tubesheet. This is expected to result in overall higher contact pressures for feedline break relative to steamline break (Reference 4-8).

For the Model F SG, referring to Figures 3-24 to 3-29 of this report, it can be observed that there is positive contact pressure for all radii of the tube bundle the entire thickness of the tubesheet during a postulated SLB (relative to NOP conditions), therefore, as the contact pressures during a postulated FLB would be expected to be higher, the effective crevice length ratio (l_{NOP}/l_{DBA}) is always less than or equal to 1.0.

4.3 C^2 MODEL LEAKAGE INTEGRITY SUMMARY

Based on Sections 4.1 and 4.2 above, it is concluded that the current licensing basis leakage factors identified in Reference 4-3 continue to apply when considering the C^2 model results.

Table 4-1 Crevice Length Subfactors Based on C^2 Model Contact Pressure Profiles

Model D5	Tube Bundle Radius (Inches)						
	4.437	10.431	18.139	26.703	42.974	49.825	
Length (NOP) inches[1]	[					]	a,c,e
Length (SLB) inches[1]	[					]	
H* Value	13.36	13.36	13.36	13.36	13.36	13.36	
Length Above H* (NOP)[2]	[					]	a,c,e
Length Above H* (SLB)[2]							
Revised (l_{NOP}/l_{SLB}) Subfactor	[					]	

[1] Length is equal to the length of positive contact pressure from the bottom of the tubesheet.
[2] Length is equal to the length of positive contact pressure above the H* distance of 13.36 inches from the top of the tubesheet.

4.4 REFERENCES

4-1 WCAP-17071-P, Revision 2, "H*: Alternate Repair Criteria for the Tubesheet Expansion Region in Steam Generators with Hydraulically Expanded Tubes (Model F)," September 2010.

4-2 WCAP-17072-P, "H*: Alternate Repair Criteria for the Tubesheet Expansion Region in Steam Generators with Hydraulically Expanded Tubes (Model D5)," May 2009.

4-3 LTR-SGMP-09-100 P-Attachment, Rev. 1 "Response to NRC Request for Additional Information on H*; Model F and Model D5 Steam Generators," September 7, 2010.

4-4 CN-SGDA-03-119, "Calculation of Loss Coefficient for Model D5 Steam Generators," Westinghouse Electric Company LLC, November 10, 2003.

4-5 STD-MCE-03-49, "Determination of Model D5 Tube-to-Tubesheet Leakage Resistance for H-star Program for CBE/CDE/DDP/TCX," November 4, 2003.

4-6 LTR-SGMP-10-95 P-Attachment, Rev. 1, "H*: Alternate Leakage Calculation Methods for H* for Situations When Contact Pressure at Normal Operating Conditions Exceeds Contact Pressures at Accident Conditions," September 2010.

4-7 Dynamic Viscosity Data from Isothermal Properties of Water, National Institute of Standards and Technology, Online Data Base, webbook.nist.gov.

4-8 LTR-SGMP-10-135 Assessment of Feedline Break Conditions on Contact Pressures for Model F for H*, 10/26/10

5 REPORT SUMMARY AND CONCLUSIONS

The purpose of this report is to provide final resolution of the NRC technical issue regarding tubesheet bore eccentricity on the H* criterion. As a result, the NRC staff asked 14 questions related to this issue. As stated in Section 1.0 of this report, the content of this report primarily focuses on resolving NRC Request for Additional Information (RAI) numbers 5 and 12. A roadmap was provided in Section 1.0 to previous documents issued by Westinghouse in response to the remainder of the 14 RAI.

1. There are two principal requirements for H*: Assure that tube(s) do not pull out of the tubesheet under the most limiting loadings during normal or accident conditions.
2. Assure that primary to secondary leakage through the tube-to-tubesheet crevice is no greater than that assumed in the final safety analysis report (FSAR) for the most limiting accident.

Concerning item 1, the Westinghouse action plan to resolve the NRC staff tube pull out concerns relating to tube bore eccentricity involved the development of a more accurate analysis model for calculating tube joint contact pressure. As discussed in Section 3.0 of this report, the square cell (C^2) model analysis is an independent method of modeling the contact pressure distribution between the tube and the tubesheet throughout the tubesheet thickness.

Consistent application of a single structural model showed that the limiting condition for the Model D5 plants is the SLB condition, rather than the NOP conditions as documented in the current licensing basis (Reference 5-4). For the Model D5 SG for the limiting plant, the value of H* inspection depth required to meet the structural integrity goals of the plant decreased by 3.59 inches; whereas, the value for the limiting plant for the Model F SGs increased by 2.1 inches. The differences between the two models are the results of different end cap loads, tubesheet displacements and contact pressure distributions. A direct comparison between the licensing basis probabilistic H* values and the square cell analysis probabilistic H* values for the Model F and Model D5 steam generators is shown in Table 5-1. The H* values provided in Table 5-1 provide tube pull out capability that meet or exceed the structural integrity acceptance criteria identified in Section 4.1 of References 5-3 and 5-4.

The impact of the new square cell model results on the existing licensing basis leak rate factors provided in Reference 5-6 for the Model F and Model D5 steam generators was evaluated. Of the four leakage subfactors identified in References 5-3 and 5-4, it was determined that the square cell model results affect two of the four subfactors for the Model D5 steam generator during the postulated SLB event. The subfactors affected are the loss coefficient subfactor (K_{NOP}/K_{SLB}) and the effective crevice length subfactor (l_{NOP}/l_{SLB}).

Relative to the loss coefficient subfactor for leakage, as discussed in Section 4.0 of this report, the licensing basis for the Model D5 SG includes a SLB condition that differs from the SLB conditions in the licensing basis for the Model F SG. The Model D5 SG SLB transient includes a significantly lower temperature; as a result, it cannot be shown that the contact pressures at accident conditions exceed those at normal operating conditions, and the NRC criterion for contact pressure ($Pc_{SLB}:Pc_{NOP}>1$) is not met, implying that a loss coefficient subfactor of 1.0 cannot be justified. This was determined to be the case using both the thick shell equation model and the C^2 model to calculate tube joint contact pressures. Consequently, it was necessary to utilize a different approach for leakage analysis that does not depend on loss coefficient being independent of contact pressure to show that the accident induced leakage value assumed in the FSAR is not exceeded.

Two alternate approaches were considered:

1. Parametric assumptions of loss coefficient dependency on contact pressure.

2. Application of parallel plate theory.

Both approaches calculated a SLB leakage factor of less than [ ]^{a,c,e} (Reference 5-2) which remains bounded by the current licensing basis factors for the H* fleet for the Model D5 SGs with considerable margin.

Relative to the effective crevice length subfactor, it has been determined that a subfactor > 1.0 exists during a postulated SLB for a Model D5 SG at certain radii. This is the case because, according to the square cell model results, positive contact pressure does not exist for the same distance above H* during normal operating and postulated SLB conditions. The length of positive contact pressure decreases during a postulated SLB event which results in a bounding leakage subfactor of [ ]^{a,c,e} (see Section 4.2.1). However, this larger subfactor is counterbalanced by the reduction in dynamic viscosity that occurs during a postulated SLB due to the greater than 250°F reduction in primary fluid temperature that occurs during the transient.

For the Model D5 SGs, the leakage factors range from 3.11 to 3.27 (References 5-6 and 5-9) for a postulated FLB heatup event. It has been confirmed that it remains conservative to apply a value 1.0 for both the leakage subfactor for loss coefficient and effective crevice length during a postulated FLB for the Model D5 SG. The results from application of the square cell model analysis verify that contact pressure increases during a postulated FLB relative to normal operating plant conditions at all tube bundle radii and elevations. It also has been verified that positive contact pressure exists at all radii and tubesheet elevations. Therefore, the leakage rate factors identified in the current licensing basis (Reference 4-3) continue to apply for the Model D5 SGs.

Finally, using either the thick shell equation or the C^2 model approach, results show that the contact pressures during SLB conditions at various elevations between 0 and 21.03 inches at all radii in the tube bundle always exceeds the contact pressures during normal operating conditions meeting the criterion (Pc_{SLB}:Pc_{NOP}>1) for the Model F SGs. Also, contact pressure is always positive at all radii and tubesheet elevations during a postulated SLB. Based on a qualitative assessment of the factors that impact contact pressures, it is concluded that contact pressure increases during a postulated FLB relative to a postulated SLB for the Model F SG. Therefore, no alternate method for leakage analysis is required and the current licensing basis leakage factor values identified in the current licensing basis (References 5-6 and 5-9) continue to apply for the Model F SGs.

Concerning all other design basis accidents that model accident condition leakage, as discussed in References 5-3 and 5-4, the design specification curves for the locked rotor and control rod ejection events apply for the leakage factors for these transients. These transients are of very short duration and the H* leakage calculations employ a time integrated leakage approach. The same leakage factors for a postulated locked rotor and control rod ejection event for the Model D5 and F SGs in the H* fleet included in the current licensing basis (References 5-6 and 5-9) continue to apply.

Based on the above, with the use the leakage factors included in the current licensing basis (References 5-6 and 5-9), it is concluded that primary to secondary leakage through the tube-to-tubesheet crevice is bounded by the values assumed in the final safety analysis report (FSAR) for the most limiting accident.

Satisfactory resolution of the NRC technical issue regarding tubesheet bore eccentricity is complete. Together with documents provided under separate cover, (e.g., Reference 5-7) this document completes the response to the RAI provided in Reference 5-8. Application of the C^2 model has provided independent confirmation that the structural criteria are met. Probabilistic H* values were re-calculated based on application of the C^2 model and substantially confirm the values contained in the current licensing basis. The differences between the H* results based on the C2 model and those from the prior application of the thick shell model are explained. The leakage factors contained in the current licensing basis for the Model D5 and Model F SGs are shown to be conservative and acceptable for implementation of H*.

Table 5-1 Results of Probabilistic Comparison Study for the Limiting Plants in the H* Fleet

			Thick Shell Calculations			Square-Cell Calculations			
			(Reference 5-5)		Implemented H* (1)	Whole Bundle		Whole Plant	
SG Model/ Limiting Plant	Limiting Operating Condition	Current Licensing Basis	95/50 Whole Bundle	95/95 Whole Plant	Plant Tech Spec	95/50	95/95	95/50	95/95
			in	in	in	in	in	in	in
Model F / Millstone 3	NOP	WCAP-17071-P	11.20	13.02	13.10	[ ]^{a,c,e}	[ ]^{a,c,e}	15.15	15.20
Model D5/ Byron & Braidwood 2	SLB	WCAP-17072-P	13.80	16.95	16.95	13.35	13.36	N/A	N/A

Notes:

(1) Values taken from utilities' 2009 license amendment requests.

5.1 REFERENCES

5-1. Not used.

5-2. LTR-SGMP-10-95 P-Attachment, Rev. 1, "H*: Alternate Leakage Calculation Methods for H* for Situations When Contact Pressure at Normal Operating Conditions Exceeds Contact Pressures at Accident Conditions," September 2010.

5-3. WCAP-17071-P, Revision 2, "H*: Alternate Repair Criteria for the Tubesheet Expansion Region in Steam Generators with Hydraulically expanded Tubes (Model F)", September 2010.

5-4. WCAP-17072-P, "H*: Alternate Repair Criteria for the Tubesheet Expansion Region in Steam Generators with Hydraulically expanded Tubes (Model D5)," May 2009.

5-5. LTR-SGMP-09-104 P-Attachment, Revision 1, "White Paper on Probabilistic Assessment of H*," August 13, 2009.

5-6. LTR-SGMP-09-100 P-Attachment, Rev. 1 "Response to NRC Request for Additional Information on H*; Model F and Model D5 Steam Generators," September 7, 2010.

5-7. LTR-SGMP-10-33 P-Attachment, "H*: Response to NRC Questions Regarding Tubesheet Bore Eccentricity," September 2010.

5-8. USNRC Letter, "Vogtle Electric Generating Plant, Units 1 and 2 – Transmittal of Unresolved Issues Regarding Permanent Alternate Repair Criteria for Steam Generators (TAC Nos. ME 1339 and ME 1340)," November 23, 2009.

5-9. USNRC Letter, "Catawba Nuclear Station, Unit 2, Issuance of Amendment Regarding the Steam Generator Program (TAC No. ME4108)," September 27, 2010.